

Knockout of mitogen-activated protein kinase 3 causes barley root resistance against *Fusarium graminearum*.

Jasim Basheer^{1†}, Pavol Vadovič^{1†}, Olga Šamajová¹, Pavol Melicher¹, George Komis¹, Pavel Křenek¹, Michaela Králová^{2#}, Tibor Pechan³, Miroslav Ovečka¹, Tomáš Takáč¹, and Jozef Šamaj^{1*}

¹Department of Biotechnology, Faculty of Science, Palacký University Olomouc, Olomouc, Czech Republic

² Department of Molecular Biology, Centre of the Region Haná for Biotechnological and Agricultural Research, Faculty of Science, Palacký University Olomouc, Czech Republic

³Institute for Genomics, Biocomputing and Biotechnology, Mississippi Agricultural and Forestry Experiment Station, Mississippi State University, Starkville, MS, United States

*Correspondence: Jozef Šamaj, jozef.samaj@upol.cz

†These authors contributed equally to this work

Present address: Laboratory of Growth Regulators, Palacký University & Institute of Experimental Botany, Czech Academy of Sciences, Olomouc, Czech Republic

ORCID Numbers:

Jasim Basheer: 0000-0001-5557-6152

Pavol Vadovič: 0000-0003-0579-3487

Olga Šamajová: 0000-0001-6121-7164s

Pavol Melicher: 0000-0003-0576-8855

George Komis: 0000-0002-6672-2722

Pavel Křenek: 0000-0002-0206-4978

Michaela Králová: 0000-0002-5273-5936

Tibor Pechan: 0000-0003-2224-7832

Miroslav Ovečka: 0000-0002-1570-2174

Tomáš Takáč: 0000-0002-1569-1305

Jozef Šamaj: 0000-0003-4750-2123

Word count: 6888

Abstract

The roles of mitogen-activated protein kinases (MAPKs) in plant-fungal pathogenic interactions are less understood in crops. Here, microscopic, phenotyping, proteomic and biochemical analyses revealed that independent TALEN-based knockout lines of *Hordeum vulgare* *MITOGEN-ACTIVATED PROTEIN KINASE 3* (*HvMPK3* KO) were resistant against *Fusarium graminearum* infection. When co-cultured with roots of the *HvMPK3* KO lines, *F. graminearum* hyphae were excluded to the extracellular space, the growth pattern of hyphae was considerably deregulated, mycelia development was less efficient and number of appressoria and their penetration potential were significantly reduced. Intracellular penetration of hyphae was preceded by the massive production of reactive oxygen species (ROS) in attacked cells of the wild type, but it was mitigated in the *HvMPK3* KO lines. Suppression of ROS production in these lines coincided with the elevated abundances of catalase and ascorbate peroxidase. Moreover, differential proteomic analysis revealed downregulation of defense-related proteins in wild type, and the upregulation of peroxidases, lipid transfer proteins, and cysteine proteases in *HvMPK3* KO lines after 24h of *F. graminearum* inoculation. Consistently with proteomic analysis, microscopic observations showed an enhanced suberin accumulation in roots of *HvMPK3* KO lines, most likely contributing to the arrested infection by *F. graminearum*. These results suggest that TALEN-based knockout of *HvMPK3* leads to the barley root resistance against *Fusarium* root rot.

Keywords: barley, *HvMPK3* TALEN knock-outs, *Fusarium graminearum*, *Fusarium* root rot, resistance, reactive oxygen species, peroxidases, suberin

Introduction

Cereals are a major food staple for the world population, however, there is a substantial reduction in the annual yield because of pathogens, weeds, temperature extremes, high salt concentrations, drought, and arid conditions (Sewelam *et al.*, 2016). Diseases caused by fungal pathogens alone are responsible for the destruction of approximately 125 million tons of crops worldwide in the last decade (Vogelgsang *et al.*, 2019).

To combat invading fungi, plants recognize microbe-associated molecular patterns (MAMPs), and damage-associated molecular patterns (DAMPs), which are essential for triggering plant immunity (Schwessinger and Zipfel, 2008). MAMPs and DAMPs elicit so-called pattern-triggered immunity (PTI), which is mediated by plant pattern recognition receptors (PRRs) (Huang *et al.*, 2016). PTI is characterized by a series of events, including signaling through protein kinase cascades, generation of reactive oxygen species (ROS), calcium ion influx, transcriptional reprogramming, cell wall appositions, and hormonal changes (Kurusu *et al.*, 2015). ROS play a dual role during plant immune responses. In addition to signaling functions (Qi *et al.*, 2017), their over-accumulation leads to the hypersensitive response, which hinders the progression of the biotrophic pathogens to the plant tissues (Camagna and Takemoto, 2018; Camejo *et al.*, 2016). In contrast, necrotrophic pathogens may benefit from nutrients provided by the damaged tissues, and thus ROS accumulation facilitates the invasion of the pathogen into the tissues (Barna *et al.*, 2012; Kámán-Tóth *et al.*, 2019).

Mitogen-activated protein kinases (MAPKs) are integrated in signaling cascades responsible for conveying signals generated by extracellular and intracellular stimuli (Komis *et al.*, 2011). In Arabidopsis and rice, there are several numbers of MAPKs described, of which mostly AtMPK3, AtMPK4, and AtMPK6 and their rice orthologues, are responsible for plant resistance against pathogens (Bigeard *et al.*, 2015; Kishi-Kaboshi *et al.*, 2010; Meng and Zhang, 2013). The signaling pathway involving AtMPK3/AtMPK6 pair is responsible for the regulation of camalexin biosynthesis (a major phytoalexin found in *Cruciferae* plants) during infection of Arabidopsis by necrotrophic fungal pathogens (Mao *et al.*, 2011). However, in the case of bacterial infection, AtMPK4 is responsible for its regulation (Bazin *et al.*, 2020). MPK3/MPK6 in different plant species also regulate hypersensitive cell death responses and the generation of reactive oxygen species (Kim and Zhang, 2004; Kroj *et al.*, 2003; Liu *et al.*, 2007; Ren *et al.*, 2002). The importance of MAPK signaling in plant-pathogen interactions is

also supported by studies of bacterial effectors, several of which target and inhibit plant MAPK cascades (Cui *et al.*, 2010; Zhang and Dong, 2007). Recently, it was shown that knock-out mutations of *HvMPK3* prepared by TALEN technology attenuated the responsiveness of barley to bacterial PAMP flagellin 22 (flg22), manifested by decreased abundance of chitinases and pathogenesis-related proteins (Takáč *et al.*, 2021).

Fusarium graminearum causes a major loss of barley yield due to head blight and root rot diseases. This fungus is considered a hemibiotrophic pathogen, living in the host plants for a short period (hours to several days), before switching to necrotrophic form, which retrieves nutrients from dead cells (Tucker *et al.*, 2021, 2019). Although *Fusarium* head blight was earlier believed as a primary disease caused by *F. graminearum*, the root colonization by this pathogen is currently recognized as very important for immense economic losses. *Fusarium* root rot causes rapid necrosis, leading to a significant reduction in root growth and biomass, which is accompanied by the progression of the pathogen to the stem base (Smiley *et al.*, 2005). The growth-inhibiting impact of the pathogen was assigned to the production of the mycotoxin deoxynivalenol (DON) (Masuda *et al.*, 2007). The hyphae colonize intra- and intercellular spaces in the root cortex in sensitive wheat cultivars, while the invasion in resistant cultivar is stopped at the epidermal cells (Wang *et al.*, 2015). Barley defense mechanisms against *Fusarium* root rot are poorly understood. So far, these resistance strategies involved *de novo* biosynthesis of barley root exudates (Lanoue *et al.*, 2010), activation of jasmonic acid (JA)-dependent defense genes and genes related to DON detoxification (Wang *et al.*, 2018). The role of MAPKs in barley responses to *Fusarium* has not been elucidated, and their participation in *Fusarium*-induced signal transduction is unknown.

In the present study, we discovered that independent barley lines with TALEN-based knock-out mutations of *HvMPK3* exhibited higher root resistance to *F. graminearum* and produced less ROS than wild type plants. *Fusarium* hyphae potential to penetrate the root cells of *HvMPK3* lines significantly decreased. This was accompanied by the attenuation of defense responses in wild type plants and the induction of upregulated levels of cysteine proteases and secretory peroxidases in *HvMPK3* KO lines, as documented by proteomic analysis. Our results indicate that ROS generation, might facilitate the invasion of wild type plants by *F. graminearum*, but elevated abundances of cytosolic ascorbate peroxidase and catalase might reduce ROS levels, thus contributing to the higher resistance of *HvMPK3* KO lines. Finally,

the stiffening of the cell walls by suberin deposition likely represents a barrier, which prevents pathogen invasion to the root cells of *HvMPK3* KO lines.

Results

Phenotype of wild type and HvMPK3 KO plants infected by Fusarium graminearum

Fungal mycelium developed extensively after infecting the roots of five days old barley seedlings by *F. graminearum* conidia. Ten days after infection, densely developed mycelium surrounded seeds and basal parts of the root system in wild type (WT) plants (Figure S1A). Roots of WT plants were largely arrested in their growth (Figure S1A, black arrows). In contrast, the root system of *HvMPK3* KO-A (Figure S1B), *HvMPK3* KO-B (Figure S1C), and *HvMPK3* KO-D (Figure S1D) lines inoculated by *F. graminearum* developed well without any visible reduction of root growth. In addition, the development of *F. graminearum* mycelia itself was inhibited, particularly around the seeds and roots (Figure S1B-D). Dark brown coloration of *F. graminearum* mycelia appeared close to the seeds and the basal parts of the root system of *HvMPK3* KO lines (Figure S1B-D). On WT genotypes, however, *F. graminearum* mycelia showed pale white color and massive coverage of infected plants (Figure S1A).

Inoculation of control seedling roots (Figure 1A-D) with *F. graminearum* spores led to their germination and subsequent colonization of roots by growing mycelia. In a period of 24 h after inoculation (Figure 1E-H), the root apex of WT plants was massively invaded by GFP-expressing *F. graminearum* hyphae (Figure 1E). However, only sparse hyphae were present on the root surface of *HvMPK3* KO lines (Figure 1F-H). Propidium iodide (PI) staining of cell walls in living cells of uninfected plants (Figure 1A-D) served as a marker of root tissue organization, while accumulation of PI in nuclei in dead cells of infected plants (Figure 1E-H) indicated their mortality after penetration by *F. graminearum* hyphae. The cell death in the epidermis of WT roots colonized by *F. graminearum* was evident (Figure 1E), while the amount of dead epidermal cells in inoculated roots of *HvMPK3* KO lines was considerably low (Figure 1F-H). The quantitative analysis of cell death rate revealed a statistically significant increase in infected WT plants. In contrast, there was no statistical difference in the number of dead root epidermal cells between uninfected plants and plants analyzed 24h after inoculation in *HvMPK3* KO lines (Figure 1I).

Examination of plants 48h after inoculation with *F. graminearum* showed that roots of WT plants were massively colonized by the fungal mycelium (Figure 1J), but mycelium was much less developed around the infected area on the root surface in *HvMPK3* KO lines (Figure 1K-M). Surprisingly, this fact was related to different growth pattern of hyphae, including considerable changes in their density, but also in the shape of developing mycelium. On the surface of WT roots, the hyphae were growing in parallel with longitudinal root axis and closely associated with the surface of root epidermal cells (Figure 1J). In contrast, hyphae were growing away of the roots and often without touching the root surface of *HvMPK3* KO lines (Figure 1K-M). In addition, mycelium developed around *HvMPK3* KO roots was malformed with unusual wavy growth pattern of hyphae, and showed changed growth direction oriented perpendicularly to the axis of elongated root epidermal cells (Figure 1K-M). Using analysis of the angular distribution of growing mycelia, we quantitatively determined a degree of anisotropy of hyphae distribution at the root surface. In the WT roots, the graph shows almost uniformly longitudinal orientation of hyphae relative to the root longitudinal axis (Figure S2A). Conversely, mycelia around root surfaces of *HvMPK3* KO lines showed more random organization (Figures S2B-S2D). Quantitative evaluation revealed higher average values for angular distribution of hyphae on WT roots (Figure S2E), suggesting a high degree of anisotropy, characterized by hyphae arrangement in one orientation. Opposite, statistically significant lowering of values determining a high degree of isotropy characterized by uniform distribution of hyphae with no prevalent orientation, was found in *HvMPK3* KO lines (Figure S2E). We also analysed fluorescence skewness, defining a pattern of fluorescence intensity distribution on the root surface and comparing how a ratio between high and low fluorescence intensities distribution is changing. This analysis revealed a high degree of fluorescence uniformity (referred by lower values) on the surface of WT roots (Figure S2F), but a high degree of non-uniformity of the fluorescence intensity distribution (characterized by distinct dark and bright fluorescent areas and referred by higher values) on the surface of *HvMPK3* KO roots (Figure S2F).

In comparison to uninfected WT plants (Figure 2A), analysis of root system phenotypes of *F. graminearum*-treated WT plants (10 days after inoculation) revealed a reddish-brown coloration and malformation of some roots (Figure 2E). However, a comparison of roots of uninfected *HvMPK3* KO lines (Figure 2B-D) with infected ones (Figure 2F-H) showed no change. Roots in the basal part of the root systems of *HvMPK3* KO lines did not exhibit a

reddish-brown coloration (Figure 2F-H). The morphology (Figure S3) and the length (Figure 2I) of roots measured 10 days after inoculation revealed that *F. graminearum* infection significantly reduced the root length in the WT plants, but there was no significant difference between control *versus* infected *HvMPK3* KO lines (Figure 2I). These data indicate insensitivity of *HvMPK3* KO plants to *F. graminearum* infection in early seedling stages, and sustained root growth without deleterious effects of the pathogen.

Growth of the mycelium on the root surface precedes the hyphae invasion to the root cells by cell wall penetration. Volumetric fluorescence visualization of GFP-expressing *F. graminearum* hyphae on the root surface allowed not only qualitatively determine the distribution and density of mycelium, but also its penetration ability. Therefore, we documented the depth of hyphal invasion by color-coded fluorescence intensity distribution along the Z-axis of imaging. In WT roots 48h after inoculation with spores, such analysis revealed formation of appressoria and infection hyphae invading the root epidermal cells. Deeper position of appressoria on cell surface and intracellular location of invading hyphae were clearly distinguished from root surface mycelium according to distinct fluorescence color-coding (Figure 3A, B). In sharp contrast, the same analysis did not reveal penetration and intracellular infection hyphae formation in the root epidermis of *HvMPK3* KO lines (Figure 3C-H). Overall microscopic analysis revealed formation of dense mycelium on the surface of WT roots, with frequent infection hyphae penetration to the root epidermal cells (Figure S4A, B). In contrary, low-density surface mycelium with different growth pattern, and no hyphae penetration in the root epidermal cells were revealed in *HvMPK3* KO lines (Figure S4C-H). Moreover, occasional *F. graminearum* appressoria developed on root surfaces of *HvMPK3* KO lines were often abnormal in shape and size (yellow arrows in Figure 3C-H). Differences in appressoria morphology between *F. graminearum* mycelium growing on the surface of WT roots (Figure 3A, B, 4A) and roots of *HvMPK3* KO lines (Figure 3C-H, 4B-D) prompted us to analyze appressoria formation capacity, which may directly influence also their penetration ability to the root epidermal cells. We have found significantly lower numbers of appressoria (Figure 4E) and penetrating hyphae (Figure 4F) on the surface of *HvMPK3* KO roots compared to the WT. Therefore, data from phenotypical analysis revealed different responses of WT and *HvMPK3* KO roots to *F. graminearum* infection.

Fusarium-induced ROS production in barley roots

ROS production in infected plant cells is associated with the early recognition of pathogen at the apoplast, and is accompanied by sudden oxidative burst (Qi *et al.*, 2017). Therefore, ROS production in roots of WT and *HvMPK3* KO lines was analysed by CM-H₂DCFDA fluorescence detection 24h after inoculation with *F. graminearum* spores. This analysis revealed a substantially higher ROS accumulation in WT (Figure 5A), compared to the *HvMPK3* KO lines (Figure 5B-D). Consequently, quantitative evaluation of the fluorescent staining levels showed that ROS accumulation was substantially higher in the infected WT roots than in infected roots of *HvMPK3* KO lines (Figure 5E). Independent spectrophotometric examination of ROS levels in the infected WT and *HvMPK3* KO lines showed results consistent with these microscopic observations (Figure S5). In WT plants, ROS production in cells attacked by fungus preceded fungal hyphae penetration (Figure 5F). Such cells in the pre-invasion stage were still alive and accumulated a high amount of ROS, while other surrounding cells with absent ROS fluorescence signal were dead (Figure 5F). In the root apex of WT plants, ROS production and accumulation occurred in cells not yet penetrated with *F. graminearum* hyphae, while in most of the root epidermal cells ROS production was not detected (Figure 5G). Based on the staining of nuclei by PI, these cells were already dead and penetrated by *F. graminearum* hyphae (Figure 5G). Conversely, only a limited number of root epidermal cells appeared dead after PI staining of *HvMPK3* KO lines 24h after inoculation with *F. graminearum* spores (Figure 5H-J). Fluorescence signal for ROS detection was not observed, which was related to the low number of *F. graminearum* hyphae growing around the roots and their minimal contact with the root epidermal cells of *HvMPK3* KO lines (Figure 5H-J).

Differential proteomic analysis

To elucidate resistance mechanisms of *HvMPK3* KO lines against *F. graminearum* at molecular level, root proteomes of WT and *HvMPK3* KO lines infected with *F. graminearum* were compared to mock controls 24h after infection.

In total, we have identified 133 differentially abundant proteins in *F. graminearum*-treated WT plants, of which 43 were upregulated and 90 were downregulated in infected *versus* control plants. In *HvMPK3* KO lines, 94 differentially abundant proteins were found, from which 47 were upregulated and the same number was downregulated in infected *versus* control plants (Tables S1 and S2). We evaluated the differential proteomes of WT and *HvMPK3* KO lines using GO annotation analysis (Figure S6-S7).

Here we compared the previously published differential proteome of *HvMPK3*-KO lines exposed to flg22 (Takáč *et al.*, 2021) with the differential proteome of the same lines treated with Fusarium. In contrast to flg22, Fusarium caused the differential abundance of lipid transfer proteins (LTPs), histone isoforms and proteins involved in reactive oxygen species regulation (Figure 6). In more detail, abundances of histone isoforms were upregulated in WT, but downregulated in *HvMPK3* KO lines treated with Fusarium (Figure 6). LTPs, a protein family affected by Fusarium but not by flg22, were distinctly affected in KO *HvMPK3* lines compared to WT (Figure 6). Putative lipid transfer-like protein DIR1 and non-specific LTP1 were upregulated while YLS3 was downregulated in infected WT lines. In *HvMPK3* KO lines, Fusarium caused upregulation of two VAS lipid transfer-like proteins and downregulation of CW21 non-specific LTP.

Concerning proteins involved in redox regulation, peptide methionine sulfoxide reductase B5, thioredoxin domain-containing protein 9 and glutathione S-transferase GSTU6 were downregulated in WT (Figure 7). Peptide methionine sulfoxide reductase B3 and glutathione S-transferase GSTU1 were negatively affected by Fusarium treatment in *HvMPK3* KO lines. Monodehydroascorbate reductase 5 (involved in ascorbate regeneration) was downregulated, while thioredoxin M2 (a chloroplastic redox buffering protein) was upregulated in *HvMPK3* KO plants (Figure 7).

Fusarium also deregulated secretory peroxidases in barley. Proteome-wide, *HvMPK3* KO lines contained five secretory peroxidases and WT only three. Notably, abundances of secretory peroxidases were decreased in WT, while three out of five secretory peroxidases were upregulated in the *HvMPK3* KO lines. Using specific activity staining on native gels, we have found that *HvMPK3* KO lines exhibited also increased activities of three peroxidase isoforms (Rf 0.63, 0.90, 0.98), as compared to the WT (Figure 8A, B). To assess the abundance of major H₂O₂-decomposing enzymes, L-ascorbate peroxidase and catalase were analyzed using immunoblot assays. We detected cytosolic APX (cAPX) in the barley root extracts employing anti-ascorbate peroxidase (APX) antibody (Figure 8C, D). Remarkably, the abundance of cAPX increased in *HvMPK3* KO lines, while it decreased in WT plants. In addition, we observed an increase of catalase abundance in both analyzed *HvMPK3* KO lines, while it slightly decreased in WT (Figure 8E, F). These results suggest that *HvMPK3* KO lines likely exert an increased capacity to decompose H₂O₂ during *F. graminearum* infection.

Moreover, cysteine proteases were more affected by *Fusarium* as by flg22. They were downregulated in WT but mostly upregulated in *HvMPK3* KO lines. Next we identified more proteins belonging to the family of heat shock proteins in the *Fusarium*-induced differential proteome. The majority of them was downregulated in *HvMPK3* KO lines.

Proteins involved in cell wall modifications and abiotic stress response were more and preferentially affected by *Fusarium* as compared to flg22, and these protein groups mostly showed reduced abundances in WT. Finally, enzymes with ubiquitination and deubiquitination activities were also affected by *Fusarium*, but without differences between WT and *KO HvMPK3* lines.

As *HvMPK3* KO lines exhibited reduced colonization of roots by *F. graminearum* hyphae, we focused on proteins predicted to be localized to extracellular space (Table S3). These included three cysteine proteinases, which were upregulated in *HvMPK3* KO lines, and downregulated in WT. Furthermore, PR proteins (PR-1, thionin 2, glucan endo-1,3-beta-glucosidase 4) were found downregulated in WT. Notably, PR-1 protein was upregulated in *HvMPK3* KO lines. Immunoblotting analysis validated this differential abundance of PR-1 in WT and *HvMPK3* KO lines (Figure 8G, H). Some of the above-mentioned LTPs were predicted as extracellular, including DIR1 putative lipid transfer-like protein, non-specific LTP1 and two VAS lipid transfer-like proteins (Table S3). LTPs together with another extracellular protein, GDSE esterase/lipase At5g33370, are involved in cutin and suberin formation in plants (Edqvist *et al.*, 2018; Hong *et al.*, 2017). Therefore, we examined suberin accumulation in roots of *F. graminearum*-treated WT and *HvMPK3* KO lines using specific fluorescent dye fluorol yellow 088. This histochemical analysis showed stronger suberin deposition to the root surface cell layers of non-infected *HvMPK3* KO lines (Figure 9B, C, G), but not in WT plants (Figure 9A, G). The suberin histochemical staining at root surface cell layers was considerably enhanced only in *HvMPK3* KO lines after *F. graminearum* infection (Figure 9D, E, F, G). In addition, the suberin staining also increased in the root endodermis and stele of *HvMPK3* KO lines (Figure 9B, C, E, F). In contrast, histochemical staining of lignin with basic fuchsin showed an opposite tendency, and no differences in lignin staining were observed under control conditions (Figure 10A-C, G). Nevertheless, treatment with *F. graminearum* caused over 54,5% decrease of lignin staining in WT roots, but only 18,5-28% decrease in *HvMPK3* KO lines (Figure 10D-G). These results suggest that a suberized cell wall barrier against *F. graminearum* invasion was built up at the surface layers of *HvMPK3* KO roots.

In conclusion, proteomic analysis showed that WT exhibited reduced abundances of PR proteins, while the resistance of *HvMPK3* KO lines to *F. graminearum* was accompanied by upregulation of PR proteins, peroxidases, LTPs, cysteine proteinases, proteins involved in suberin formation and it was corroborated by overabundances of cAPX and catalase.

Discussion

The diversified family of MAPKs lies in the core of plant defense mechanisms due to their significant role in extracellular stimuli perception. In addition, MAPK cascades are responsible for plant resistance to abiotic stresses and exert multiple developmental functions (Bigéard *et al.*, 2015; Komis *et al.*, 2018). Despite a significant number of MAPK-related studies in dicots like *Arabidopsis*, the current understanding of MAPK roles in defense of cereal crops against pathogens is still limited. In cereals, MAPKs play either positive or negative roles in immune reactions against fungal pathogens (Křenek *et al.*, 2015; Chen *et al.*, 2021). In rice, the OsMKK4–OsMPK3/OsMPK6 module participates in transduction of a fungal chitin elicitor signal and regulates defense responses leading to the biosynthesis of diterpenoid phytoalexins and lignin, and progression of plant cell death (Kishi-Kaboshi *et al.*, 2010). OsMPK3 negatively regulates the expression of defense genes and the defense reactions against hemibiotrophic blast fungus *Magnaporthe grisea* (Xiong and Yang, 2003). It was reported that this negative regulation is mediated through interaction with, and by phosphorylation of OsMPK3 via calcium-dependent protein kinase OsCPK18 (Xie *et al.*, 2014). Wheat TaMPK3, unlike TaMPK6, is specifically activated, and its transcript levels as well as abundance are increased during compatible interactions with necrotrophic fungus *Mycosphaerella graminicola* (Rudd *et al.*, 2008). This increase is directly correlated with the onset of programmed cell death (PCD) and the generation of related PCD symptoms (Rudd *et al.*, 2008). Barley *MPK3* is upregulated in response to the rust fungus *Puccinia hordei* inoculation, especially during effector-triggered immunity (Křenek *et al.*, 2015). Remarkably, *HvMPK3* KO lines showed attenuated response to flg22 treatment in terms of defense-related genes such as chitinases, indicating some positive role of *HvMPK3* in PTI (Takáč *et al.*, 2021).

Although Fusarium root rot is capable to cause severe yield losses, the plant defense mechanism against this disease has not been sufficiently investigated and understood yet. Role of MAPKs in cereal responses to Fusarium were not studied before. The resistance against

Fusarium root rot was previously shown to be mediated by hindering the penetration of the fungi at the wheat epidermal cells (Wang *et al.*, 2015). Our results suggest that the exclusion of *F. graminearum* to the extracellular space in the roots of *HvMPK3* KO lines is likely caused by suberin deposition to the root surface of these lines, which is also supported by upregulation of proteins involved in suberin formation. We also observed decrease in lignin deposition, similarly as previously published for *F. oxysporum* treatment of flax and *F. solani* treatment of soybean (Lozovaya *et al.*, 2006; Wojtasik *et al.*, 2016).

When compared to flg22 treatment (Takáč *et al.*, 2021), *F. graminearum* infection had more obvious impact on the barley proteome, especially concerning changed abundance of extracellular proteins. This might be assigned to the hemibiotrophic pathosystem of the fungus, eliciting more complex defense mechanisms compared to bacterial elicitor flg22. Hence, this proteomic analysis allowed to gain a more detailed insight into defense mechanisms occurring in *HvMPK3* KO lines and suggested that WT roots were compromised in defense response, most likely due to fungus-secreted toxin effectors. It was illustrated by the downregulation of PR17c precursor and several isoforms of cysteine proteases, representing well-known pathogen effector targets (Zhang *et al.*, 2012, Mueller *et al.*, 2013). Cysteine proteases are major regulators of plant defense responses (Misas-Villamil *et al.*, 2016) and in contrast to WT, their abundance considerably increased in *HvMPK3* KO lines, indicating that they might mediate resistance of these lines against *F. graminearum*.

Specialized infection structures called appressoria are necessary for the *F. graminearum* infection. It was reported on plants like wheat, rice, corn or barley attacked by different fungal pathogens, including rusts, powdery mildew and blast diseases (Boenisch and Schäfer 2011; Qiu *et al.*, 2019). To facilitate host penetration, appressoria of *Magnaporthe oryzae*, generate enormous pressure up to 8.0 MPa that drive physical rupture of the host cell wall (Talbot, 2019). *F. graminearum* can produce multicellular appressoria called infection cushions (Boenisch and Schäfer 2011), whereas the biology of these structures is not completely known. Here, the number of formed and invading appressoria were significantly higher in the case of WT as compared to the *HvMPK3* KO lines. Twenty-four hours after infection, fungal hyphae successfully invaded the epidermal root cells of WT plants, which was preceded by the dramatic ROS increase and accumulation, leading to hyphae penetration to cells. This is entirely consistent with the previously described model of hemibiotrophic and necrotrophic fungal pathosystems (Desmond *et al.*, 2008). In contrast, the production of ROS

was substantially lower in infected *HvMPK3* KO plants, partly due to prevention of the interaction between the pathogen and the root surface of transgenic plants, and partly also due to their elevated antioxidant capacity mediated by cytosolic ascorbate peroxidase and catalase.

The ROS generated and released during infection can affect both counterparts, the host and the microbe (Desmond *et al.*, 2008; Yang and Fernando, 2021). ROS are indispensable for the activation of plant defense responses as a signaling component (Lee *et al.*, 2020) or they can cause peroxidation of lipids, oxidation of proteins, damage to nucleic acids, enzyme inhibition, and activation of PCD pathway during hypersensitive response (Camagna and Takemoto, 2018), thus leading to the inhibition of biotrophic pathogens. However, the *Fusarium* infection represents another example, since ROS accumulation is induced by its toxins in the host plants (Desmond *et al.*, 2008). *Fusarium* infection follows the H₂O₂ produced by the host cells, which causes enhanced production of fungal toxins enabling hyphae penetration into the host cells (Khaledi *et al.*, 2016).

Secretory peroxidases were one of the most affected protein groups in both *HvMPK3* KO and WT lines after *F. graminearum* infection. All peroxidase isoforms were downregulated in WT, but three out of five peroxidases were upregulated in *HvMPK3* KO lines in response to *F. graminearum*. Secretory peroxidases belong to class III of plant peroxidases, having a broad spectrum of activities in plants (Almagro *et al.*, 2009; Passardi *et al.*, 2005; Sasaki *et al.*, 2004). Such peroxidases belong to a PR protein 9 subfamily and are supposed to reduce the progression of pathogens by a generation of structural barriers. They are bifunctional because they exert either ROS-scavenging or ROS-producing activity (Passardi *et al.*, 2004). Peroxidase activity contributes to the ROS generated during oxidative burst (O'Brien *et al.*, 2012). ROS produced by peroxidases may either have signaling roles or contribute to the toxic environment for the pathogen (Camejo *et al.*, 2016).

One of the crucial features of secretory peroxidases is to mediate cross-linking of cell wall components leading to cell wall reinforcement. They may cross-link extensins leading to the formation of large oligomers (Mishler-Elmore *et al.*, 2021). The cross-linking of ferulic acid by covalent bonds requires the presence of cell wall peroxidases. Such cross-linked ferulic acid may create intra- or inter-polysaccharide bonds leading to cell wall stiffening (Fry, 2004). Lignin formation depends on oxidative cross-linking of monolignols (Ralph *et al.*, 2004) and expression of peroxidases was shown to correlate with lignification (Cosio *et al.*, 2017; Sorokan *et al.*, 2014). Similarly, suberin poly-phenolic domain assembly requires peroxidase

mediated oxidative coupling reactions (Bernards *et al.*, 2004). Moreover, transient overexpression of *HvPrx40* a class III peroxidase in barley epidermis, improves resistance against *Blumeria graminis* f.sp. *hordei* pathogen (Johrde and Schweizer, 2008). It is likely that peroxidases similar to peroxidase 12 (*Arabidopsis thaliana*), cationic peroxidase PNC1 (*Arachis hypogaea*), and peroxidase HRPN (*Armoracia rusticana*) contribute to the formation of suberized structural barriers which exclude *F. graminearum* to the extracellular space in *HvMPK3* KO plants. Moreover, a genomic study reported a possible link of GDSL esterase/lipases to suberin biosynthesis (Soler *et al.*, 2007). Protein similar to GDSL esterase/lipase At5g33370 (*Arabidopsis thaliana*) was significantly upregulated in *HvMPK3* KO plants. According to our results, *HvMPK3* KO lines activated a different set of LTPs compared to WT. A protein similar to lipid transfer-like protein VAS, implicated in suberin formation in *Arabidopsis* (Edstam *et al.*, 2013), was upregulated in *HvMPK3* KO lines. Also, Pitzschke *et al.*, (2014) found that AZI1 (belonging LTPs) directly interacts with AtMPK3, and confers salinity tolerance in *Arabidopsis* (Pitzschke *et al.*, 2014). In summary, our results indicate that the cell wall stiffening by suberin in surface root cells might substantially contribute to the resistance of *HvMPK3* KO lines against *F. graminearum*. This might suggest a connection between *HvMPK3* and LTPs as a part of barley defense mechanism against *F. graminearum* infection.

Since TALEN-based knockout of *HvMPK3* causes resistance to *F. graminearum* it provides a reliable tool for targeted biotechnological application in important cereal crop such as barley.

Experimental procedures

Cultivation of plant material

Three independent homozygous knock-out lines of barley (*Hordeum vulgare* L.) designated as *HvMPK3* KO-A, *HvMPK3* KO-B and *HvMPK3* KO-D, and control WT lines (Takáč *et al.*, 2021) were used for the experiments. Seeds were surface sterilized using 5% (v/v) sodium hypochlorite and 70% (v/v) ethanol, followed by an additional incubation with 500 mM (v/v) H₂O₂ overnight. After sterilization, the seeds were imbibed and stratified on plates with agar-solidified nitrogen-free Fahræus medium (Fåhræus, 1957) at 4°C for synchronous germination (Perrine-Walker *et al.*, 2007). The stratified sterile seeds on plates were transferred

to phytotron (Weiss-Gallenkamp, Loughborough, United Kingdom) and cultivated at 21°C for 16 h in the light (day), and 8 h in darkness (night), 70% relative humidity with light levels of 150 $\mu\text{mol}\cdot\text{m}^{-2}\cdot\text{s}^{-1}$ provided by cool white fluorescent tubes (Philips Master tl-d 36W/840).

Preparation of fluorescent F. graminearum

Mycelia of *F. graminearum* were cultivated in Mung bean soup (140 rpm, 20°C, 3 days), subsequently filtered through glass wool and centrifuged (300 rpm, room temperature, 5 min). Conidia obtained as such, were resuspended in sterile distilled water and inoculated on yeast extract-peptone-dextrose (YPD) medium. After overnight cultivation (180 rpm, 30°C), the mycelium was filtered through Miracloth (Merck) and washed with sterile distilled water, and 1.2 M KCl. For protoplast isolation, mycelia were cultivated in a solution containing 250 mg driselase, 1 mg chitinase, and 100 mg lysing enzyme from *Trichoderma harzianum* (all from Sigma-Aldrich). After 3 h (90 rpm, 30 °C), the enzyme-protoplast solution was run over the frit and the flow-through was centrifuged (3000 rpm, 4 °C, 10 min). Obtained pellet was washed with 1.2 M KCl, then resuspended in STC buffer (1.2 M sorbitol, 50 mM CaCl₂).

Plasmid (5 μg of *pNDN-OGG* containing *GFP*; Schumacher, 2012) was mixed with 2x STC buffer, *F. graminearum* protoplasts, and 50% (w/v) polyethylene glycol (PEG) 4000. After 25 min on ice, 50% (w/v) PEG 4000 was added. Next, the mixture was incubated 10 min at RT, followed by addition of 1x STC buffer. Prepared samples were mixed with Regeneration agar containing nourseothricin (300 $\mu\text{g}\cdot\text{ml}^{-1}$, Jena BioScience, *pNDN-OGG*) or hygromycin (100 $\mu\text{g}\cdot\text{ml}^{-1}$, InvivoGen, *pNDH-OCT*). After 5 days at 20 °C, nourseothricin- and hygromycin-resistant transformants were transferred into complete medium (CM) agar plates containing antibiotics in the final concentration of 100 $\mu\text{g}\cdot\text{ml}^{-1}$.

Genomic DNA was extracted from lyophilized *F. graminearum* mycelia according to Cenis, (1992). Diagnostic PCR was performed using GoTaq G2 Flexi DNA polymerase according to a manufacturer's protocol (Promega). Primers were designed using Primer3 0.4.0 software and synthesized by Sigma-Aldrich. The presence of *pNDN-OGG* or *pNDH-OCT* in *F. graminearum* transformants was checked with primers PoliC_fw (5'-CCCGGAAACTCAGTCTCCTT-3') and TgluC_rev (5'-GTCTTCCGCTAAAACACCCC-3') (1,295 bp) or PoliC_fw and Ttub_rev (5'-GAGGTGTGAGCATGGAAGTGATG-3') (1,593 bp), respectively.

Homokaryots of *OE:GFP* transformants were obtained by single spore isolation. Briefly, fungi were cultivated in Mung bean soup (20°C, 140 rpm) and after 5 days, the cultures were filtered through glass wool and centrifuged (10 min, 3000 rpm, 4°C). Obtained conidia were resuspended in sterile distilled water and sprayed onto CM agar plates containing appropriate antibiotics in the final concentration of 100 µg/ml.

Infection of barley plants with Fusarium

Fusarium grown in potato dextrose agar (PDA) medium for 2 weeks at 28 °C was washed with sterile distilled water containing 0.01% (v/v) Tween and filtered through sterile miracloth to obtain conidial spores ($\sim 1 \times 10^5$ spores.ml⁻¹) (Erayman *et al.*, 2015). Five days old barley seedlings were infected by dipping in freshly prepared conidial suspension (sterile distilled water containing 0.01% (v/v) Tween was used as control) and put back to the media for incubation for further experiments. Microscopic, biochemical and proteomic analyses were performed on control and *Fusarium*-treated plants 24h and 48h post-infection.

Phenotypic and microscopic analysis

For microscopic analysis, the roots of both WT and *HvMPK3* KO plants 24h and 48h after inoculation with GFP-labeled *F. graminearum* were used. Infected plants were grown in microscopic growth chambers (Nunc™ Lab-Tek™ II Chambered Coverglass (Thermofischer scientific, USA)) and observed using 488 nm excitation for GFP and the 517-527 nm emission using confocal laser scanning microscope LSM710 (Carl Zeiss, Germany). The images were color-coded for the analysis of the penetration of the infection hyphae in root epidermal cells using appropriate Zen Blue software function. The numbers of appressoria and penetration events were counted from the images and were compared among the lines by one-way ANOVA test at significance level at $p < 0.05$. Roots were stained with PI (1 mg.ml⁻¹) for 10 min, washed with liquid Fahræus medium for 1 min, and observed under spinning disk microscope (Carl Zeiss, Germany) equipped with Plan-Apochromat 20×/0.8 NA (Carl Zeiss, Germany) at 488 nm (for GFP) and 561 nm (for PI) with emission filters BP525/50 (for GFP) and BP629/62 (for PI). Image post-processing was done using ZEN 2014 software (Carl Zeiss, Germany), and the percentage of the dead cells were calculated from the processed images using the formulae (Number of dead cells / total number of cells in the field) × 100. To document root length, both treated and untreated plants were photographed by camera once per day for 10 days after the

root inoculation with GFP-labeled *F. graminearum* spores. The experiment was performed in three biological replicates. Ten plants were used per replicate and treatment for each line. The statistical significance of treatment vs. control was deemed by one-way ANOVA test at significance level at $p < 0.05$.

ROS staining

Control plants and treated plants from individual lines were used for ROS analysis 24 hrs post-inoculation with GFP-labeled *F. graminearum* using the modified protocol of Kristiansen *et al.*, (2009). Mock-treated and infected roots of WT and *HvMPK3* KO plants were incubated in 30 μM 2',7'-dichlorodihydrofluorescein diacetate (CM-H₂DCFDA; Cat no. C6827, Invitrogen™, USA) and PI (1 mg.ml⁻¹) diluted in Fahräeus medium. Seedlings in microscopic chambers were stained by perfusion, followed by incubation in darkness for 15 min. After incubation the residual stain was washed using sterile Fahräeus medium for 3 times using perfusion. After washing, the signal excited at 488 nm for ROS/GFP and 543 nm for PI was recorded at the emission range 517-527 nm for ROS/GFP and 610-625 nm (For PI) using confocal laser scanning microscope LSM710 (Carl Zeiss, Germany). The imaging of ROS accumulation in whole root was performed after staining with H₂DCFDA using epifluorescence microscope Zeiss Axio Imager M2 (Carl Zeiss, Germany) with settings for GFP excitation and emission. ROS levels in roots were analyzed semi-quantitatively from the images with ZEN software (Carl Zeiss, Germany).

Histochemical detection of suberin and lignin

Root segments (first 25 mm from the root apex) of WT and *HvMPK3* KO plants 24 h after inoculation with *F. graminearum* were used for suberin and lignin histochemical detection. Suberin and lignin staining was carried out according to a previously published protocol (Sexauer *et al.*, 2021; Ursache *et al.*, 2018). Freehand cross-sections of fixed and cleared root segments were made in the root region between 15 and 25 mm from the root apex and stained with 0,01% (v/v) Fluorol Yellow 088 in absolute ethanol (stock solution: 1% (w/v) Fluorol Yellow in DMSO) for 30 min. For lignin detection root sections were stained with 0,2% (w/v) Basic Fuchsin in ClearSee solution for overnight. Stained cross-sections of roots were observed under confocal laser scanning microscope LSM710 (Carl Zeiss, Germany) using following settings for suberin: excitation: 488 nm, detection: 500-550 nm and for lignin: excitation: 561

nm, detection: 600-650. Measurement of fluorescence intensity and post-processing were done using ZEN 2014 software (Carl Zeiss, Germany). Fluorescence mean intensities were calculated from a minimum of three biological replicates.

Western Blot Analysis

Samples were prepared and western blots performed as described before (Takáč *et al.*, 2021). Polyvinylidene difluoride (PVDF) membranes were incubated with rabbit primary anti-L-ascorbate peroxidase antibody (#AS 08 368), diluted 1:2000, or with rabbit primary anti-catalase antibody (#AS 09 501), diluted 1:2000, or with rabbit primary anti-PR-1 antibody (#AS 10 687, all from Agrisera, Sweden), diluted 1:2000, all in 1% (w/v) BSA in TBS-T at 4°C overnight. Membranes were washed thoroughly and subsequently incubated at room temperature with corresponding HRP-conjugated secondary antibody (Thermo Fisher Scientific), diluted 1:5000 in 1% (w/v) BSA in TBS-T for 1.5 h. Following three washing steps, membranes were incubated with commercial Clarity Western ECL Substrate (BioRad, Hercules, CA, United States) and documented in a ChemiDoc MP imaging system (BioRad). Experiments were performed in three biological replicates, and the statistical significance was evaluated using Student's t test ($p < 0.05$).

Analysis of peroxidase activities and spectrophotometric measurement of ROS

Specific activities of peroxidases were analyzed using staining on native PAGE gels as published previously (Takáč *et al.*, 2016). ROS levels were estimated in water extracts using xylenol orange assay as described in Takáč *et al.*, (2014). The analyses were carried out in three biological replicates on control and Fusarium-treated roots of WT and *HvMPK3* KO seedlings 24h post-inoculation. The statistical significance was evaluated using Student's t test ($p < 0.05$).

Relative protein quantitation using nano-Liquid Chromatography-Tandem Mass Spectrometry Analysis (nLC-MSMS)

Barley WT, and *HvMPK3* KO lines A, B, and D were used for proteomic study. Root parts from four plants of each line in control and treatment variants were pooled into one sample. Each sample was analyzed in two biological replicates, and the final differential proteomes of

WT and *HvMPK3* KO lines were obtained by comparing 6 biological replicates of Fusarium-treated lines vs. corresponding mock controls. Proteins were extracted using phenol extraction and methanol/ammonium acetate precipitation, as described previously (Takáč *et al.*, 2017). Total of 50 µg of proteins dissolved in 50 µl of 6 M urea were subjected to in-solution trypsin digestion.

The peptides were then cleaned on C18 cartridges (Bond Elut C18; Agilent Technologies, Santa Clara, CA), dried using SpeedVac, and utilized for nLC-MS/MS (Takáč *et al.*, 2017).

Two micrograms of protein tryptic digest were analyzed as published previously (Takáč *et al.*, 2021), using the Ultimate 3000 nano-LC system and LTQ-Orbitrap Velos mass spectrometer (both Thermo Fisher Scientific). All raw and results files were deposited to a publicly accessible database (see Data Availability Statement for details). Protein identification and label-free quantification was performed by the Proteome Discoverer 2.1 (Thermo Fisher Scientific), and an in-house script based on precursor ion intensities, as described before (Takáč *et al.*, 2021). Statistically significant results were filtered with ANOVA $p \leq 0.05$, applied to proteins exhibiting the fold change ≥ 1.5 .

Proteins identified by single peptide were excluded from the results. Proteins present in all six replicates corresponding to the control proteome, and absent in all the treated replicates were considered unique for the control proteome, and *vice versa*.

The differential proteomes were evaluated by gene ontology (GO) annotation analysis and screening of protein domains using OmixBox Functional analysis module, as specified previously (Takáč *et al.*, 2021).

Acknowledgement

We would like to thank Lena Studt from Department of Applied Genetics and Cell Biology, University of Natural Resources and Life Sciences, Vienna for helping us with *F. graminearum* transformation. We also thank technicians Petra Trčková, Pavlína Floková, Katarína Takáčová and Monika Vadovičová for their expert technical help in all stages of the presented work.

Supporting Information

Figure S1. Colonization of roots in barley plants of WT and *HvMPK3* KO lines by *Fusarium graminearum* mycelia 10 days after inoculation with spores.

Figure S2. Characterization of distribution and growth pattern of *F. graminearum* hyphae in regard of the root longitudinal axis. **(A-D)** Cytospectre graphs showing a distribution pattern of fluorescent hyphae on the root surface of WT **(A)**, *HvMPK3* KO-A **(B)**, *HvMPK3* KO-B **(C)** and *HvMPK3* KO-D **(D)** lines. **(E)** Quantitative assessment of anisotropy characterizing angular distribution of growing hyphae. **(F)** Quantitative assessment of fluorescence distribution skewness of hyphae on the surface of measured root area. Data are represented as mean \pm SD; n = 10 images/line, error bars represent standard deviations. Different lowercase letters above the error bars represent statistical significance according to one-way ANOVA and subsequent LSD test at p value < 0.05 .

Figure S3. Comparison of root phenotypes in barely WT and *HvMPK3* KO lines between non-treated and *Fusarium graminearum*-treated plants 10 days after inoculation with spores.

Figure S4. Fluorescence visualization of *F. graminearum* hyphae distribution on root surface of barley wild type (WT) and *HvMPK3* KO lines 48h after inoculation with spores. **(A, B)** WT root. **(C, D)** Root of *HvMPK3* KO-A line. **(E, F)** Root of *HvMPK3* KO-B line. **(G, H)** Root of *HvMPK3* KO-D line. Orthogonal view depicting root surface cell layers **(A, C, E, G)** and maximum intensity projection of the root surface **(B, D, F, H)**. Appressoria are indicated by asterisk and infection hyphae penetrating root epidermal cells are indicated by white arrows. Scale bars: 20 μ m **(A-H)**.

Figure S5. Concentration of hydrogen peroxide in roots of WT and *HvMPK3* KO lines 24h after inoculation with *Fusarium graminearum* spores as examined by Xylenol orange assay.

Figure S6. Comparison of gene ontology annotation according to biological processes, carried out in differential proteomes of WT and *HvMPK3* KO plants treated by *Fusarium graminearum* for 24h.

Figure S7. Comparison of gene ontology annotation according to cellular compartments, carried out in differential proteomes of WT and *HvMPK3* KO plants treated by *Fusarium graminearum* for 24h.

Figure S8. Full scan of the entire original gel whose fragments are presented in Figure 8A.

Figure S9. Full scan of the entire original blot (A) and loading control (B) whose fragments are presented in Figure 8C.

Figure S10. Full scan of the entire original blot (A) and loading control (B) whose fragments are presented in Figure 8E.

Figure S11. Full scan of the entire original blot (A) and loading control (B) whose fragments are presented in Figure 8G. The highlighted regions show sections presented in Figure 8G.

Table S1. Summary and quantification details of differentially regulated proteins found in roots of wild type plants 24h after the treatment with *Fusarium graminearum*

Table S2. Summary and quantification details of differentially regulated proteins found in roots of HvMPK3 KO plants 24h after the treatment with *Fusarium graminearum*

Table S3. Proteins predicted to be localized in extracellular space.

Funding

This work was funded by ERDF project Plants as a tool for sustainable global development (CZ.02.1.01/0.0/0.0/16_019/0000827), and NIH MS-IDeA Network of Biomedical Research Excellence award 5P20GM103476-19. The mass spectrometry proteomics analysis was performed at the Institute for Genomics, Biocomputing and Biotechnology, Mississippi State University, with partial support from Mississippi Agricultural and Forestry Experiment Station.

Authors contributions

JB, PV and MO conducted phenotypic and microscopic documentation and analysis. PV, TT and TP performed proteomics analysis. PV and PM conducted immunoblot analysis, native electrophoresis and spectrophotometric measurements. OŠ performed suberin and lignin staining and related microscopic observations and evaluation. PK selected *HvMPK3* KO and WT barley lines. MK performed *Fusarium* transformation. JB, PV, MO, TT, GK and JŠ drafted the manuscript with input from all co-authors. JŠ conceived and supervised the project, provided infrastructure and secured funding.

Data availability

The mass spectrometry proteomics data have been deposited to the ProteomeXchange Consortium via the PRIDE partner repository with the dataset identifier PXD029964".

Reviewer account details: Username: reviewer_pxd029964@ebi.ac.uk, Password: t4gfjKBY

References

- Almagro L, Gómez Ros LV, Belchi-Navarro S, Bru R, Ros Barceló A, Pedreño MA** (2009) Class III peroxidases in plant defence reactions. *J Exp Bot* **60**: 377–390
- Barna B, Fodor J, Harrach BD, Pogány M, Király Z** (2012) The Janus face of reactive oxygen species in resistance and susceptibility of plants to necrotrophic and biotrophic pathogens. *Plant Physiol Biochem* **59**: 37–43
- Bazin J, Mariappan K, Jiang Y, Blein T, Voelz R, Crespi M, Hirt H** (2020) Role of MPK4 in pathogen-associated molecular pattern-triggered alternative splicing in Arabidopsis. *PLoS Pathog* **16**: e1008401
- Bernards MA, Summerhurst DK, Razem FA** (2004) Oxidases, peroxidases and hydrogen peroxide: The suberin connection. *Phytochem Rev* **3**: 113–126
- Bigeard J, Colcombet J, Hirt H** (2015) Signaling Mechanisms in Pattern-Triggered Immunity (PTI). *Mol Plant* **8**: 521–539
- Boenisch MJ, Schäfer W** (2011) *Fusarium graminearum* forms mycotoxin producing infection structures on wheat. *BMC Plant Biol* **11**: 110
- Camagna M, Takemoto D** (2018) Hypersensitive Response in Plants. In: eLS, John Wiley & Sons, Ltd, pp. 1–7. Wiley
- Camejo D, Guzmán-Cedeño Á, Moreno A** (2016) Reactive oxygen species, essential molecules, during plant-pathogen interactions. *Plant Physiol Biochem* **103**: 10–23
- Cenis JL** (1992) Rapid extraction of fungal DNA for PCR amplification. *Nucleic Acids Res* **20**: 2380
- Chen J, Wang L, Yuan M** (2021) Update on the Roles of Rice MAPK Cascades. *Int J Mol Sci* **22**: 1–14
- Cosio C, Ranocha P, Francoz E, Burlat V, Zheng Y, Perry SE, Ripoll JJ, Yanofsky M, Dunand C** (2017) The class III peroxidase PRX17 is a direct target of the MADS-box

- transcription factor AGAMOUS-LIKE15 (AGL15) and participates in lignified tissue formation. *New Phytol* **213**: 250–263
- Cui H, Wang Y, Xue L, Chu J, Yan C, Fu J, Chen M, Innes RW, Zhou JM** (2010) *Pseudomonas syringae* effector protein AvrB perturbs Arabidopsis hormone signaling by activating MAP kinase 4. *Cell Host Microbe* **7**: 164–175
- Desmond OJ, Manners JM, Stephens AE, Maclean DJ, Schenk PM, Gardiner DM, Gardiner DM, Munn AL, Kazan K** (2008) The Fusarium mycotoxin deoxynivalenol elicits hydrogen peroxide production, programmed cell death and defence responses in wheat. *Mol Plant Pathol* **9**: 435–445
- Edqvist J, Blomqvist K, Nieuwland J, Salminen TA** (2018) Plant lipid transfer proteins: are we finally closing in on the roles of these enigmatic proteins? *J Lipid Res* **59**: 1374–1382
- Edstam MM, Blomqvist K, Eklöf A, Wennergren U, Edqvist J** (2013) Coexpression patterns indicate that GPI-anchored non-specific lipid transfer proteins are involved in accumulation of cuticular wax, suberin and sporopollenin. *Plant Mol Biol* **83**: 625–649
- Erayman M, Turktas M, Akdogan G, Gurkok T, Inal B, Ishakoglu E, Ilhan E, Unver T** (2015) Transcriptome analysis of wheat inoculated with *Fusarium graminearum*. *Front Plant Sci* **6**: 867
- Fahraeus G** (1957) The infection of clover root hairs by nodule bacteria studied by a simple glass slide technique. *J Gen Microbiol* **16**: 374–381
- Fry SC** (2004) Oxidative coupling of tyrosine and ferulic acid residues: Intra- and extra-protoplasmic occurrence, predominance of trimers and larger products, and possible role in inter-polymeric cross-linking. *Phytochem Rev* **3**: 97–111
- Hong L, Brown J, Segerson NA, Rose JKC, Roeder AHK** (2017) CUTIN SYNTHASE 2 maintains progressively developing cuticular ridges in Arabidopsis sepals. *Molec Plant* **10**: 560-574
- Huang J, Yang M, Lu L, Zhang X** (2016) Diverse Functions of Small RNAs in Different Plant–Pathogen Communications. *Front Microbiol* **4**:1552
- Johrde A, Schweizer P** (2008) A class III peroxidase specifically expressed in pathogen-attacked barley epidermis contributes to basal resistance. *Mol Plant Pathol* **9**: 687-696

- Kámán-Tóth E, Dankó T, Gullner G, Bozsó Z, Palkovics L, Pogány M** (2019) Contribution of cell wall peroxidase- and NADPH oxidase-derived reactive oxygen species to *Alternaria brassicicola*-induced oxidative burst in *Arabidopsis*. *Mol Plant Pathol* **20**: 485–499
- Khaledi N, Taheri P, Falahati-rastegar M** (2016) Reactive oxygen species and antioxidant system responses in wheat cultivars during interaction with *Fusarium* species. *Austral Plant Pathol* **45**: 653–670
- Kim CY, Zhang S** (2004) Activation of a mitogen-activated protein kinase cascade induces WRKY family of transcription factors and defense genes in tobacco. *Plant J* **38**: 142–151
- Kishi-Kaboshi M, Okada K, Kurimoto L, Murakami S, Umezawa T, Shibuya N, Yamane H, Miyao A, Takatsuji H, Takahashi A et al.** (2010) A rice fungal MAMP-responsive MAPK cascade regulates metabolic flow to antimicrobial metabolite synthesis. *Plant J* **63**: 599–612
- Komis G, Illés P, Beck M, Šamaj J** (2011) Microtubules and mitogen-activated protein kinase signalling. *Curr Opin Plant Biol* **14**: 650–657
- Komis G, Šamajová O, Ovečka M, Šamaj J** (2018) Cell and Developmental Biology of Plant Mitogen-Activated Protein Kinases. *Annu Rev Plant Biol* **69**: 237–265
- Kristiansen KA, Jensen PE, Møller IM, Schulz A** (2009) Monitoring reactive oxygen species formation and localisation in living cells by use of the fluorescent probe CM-H2DCFDA and confocal laser microscopy. *Physiol Plant* **136**: 369–383
- Kroj T, Rudd JJ, Nürnberger T, Gäbler Y, Lee J, Scheel D** (2003) Mitogen-activated protein kinases play an essential role in oxidative burst-independent expression of pathogenesis-related genes in parsley. *J Biol Chem* **278**: 2256–2264
- Křenek P, Niks RE, Vels A, Vyplelová P, Šamaj J** (2015) Genome-wide analysis of the barley MAPK gene family and its expression patterns in relation to *Puccinia hordei* infection. *Acta Physiol Plant* **37**: 1-16
- Kurusu T, Kuchitsu K, Tada Y** (2015) Plant signaling networks involving Ca²⁺ and Rboh/Nox-mediated ROS production under salinity stress. *Front Plant Sci* **6**: 427
- Lanoue A, Burlat V, Henkes GJ, Koch I, Schurr U, Röse USR** (2010) De novo biosynthesis of defense root exudates in response to *Fusarium* attack in barley. *New Phytol* **185**: 577–

588

- Lee D, Lal NK, Lin ZJD, Ma S, Liu J, Castro B, Toruño T, Dinesh-Kumar SP, Coaker G** (2020) Regulation of reactive oxygen species during plant immunity through phosphorylation and ubiquitination of RBOHD. *Nat Commun* **11**: 1838
- Liu Y, Ren D, Pike S, Pallardy S, Gassmann W, Zhang S** (2007) Chloroplast-generated reactive oxygen species are involved in hypersensitive response-like cell death mediated by a mitogen-activated protein kinase cascade. *Plant J* **51**: 941–954
- Lozovaya VV, Lygin AV, Zernova OV, Li S, Widholm JM, Hartman GL** (2006) Lignin Degradation by *Fusarium solani* f. sp. *glycines*. *Plant Dis* **90**: 77–82
- Mao G, Meng X, Liu Y, Zheng Z, Chen Z, Zhang S** (2011) Phosphorylation of a WRKY transcription factor by two pathogen-responsive MAPKs drives phytoalexin biosynthesis in *Arabidopsis*. *Plant Cell* **23**: 1639–1653
- Masuda D, Ishida M, Yamaguchi K, Yamaguchi I, Kimura M, Nishiuchi T** (2007) Phytotoxic effects of trichothecenes on the growth and morphology of *Arabidopsis thaliana*. *J Exp Bot* **58**: 1617–1626
- Meng X, Zhang S** (2013) MAPK cascades in plant disease resistance signaling. *Annu Rev Phytopathol* **51**: 245–266
- Misas-Villamil JC, van der Hoorn RAL, Doehlemann G** (2016) Papain-like cysteine proteases as hubs in plant immunity. *New Phytol* **212**: 902–907
- Mishler-Elmore JW, Zhou Y, Sukul A, Oblak M, Tan L, Faik A, Held MA** (2021) Extensins: Self-Assembly, Crosslinking, and the Role of Peroxidases. *Front Plant Sci* **12**: 664738
- Mueller AN, Ziemann S, Treitschke S, Aßmann D, Doehlemann G** (2013) Compatibility in the *Ustilago maydis*–Maize Interaction Requires Inhibition of Host Cysteine Proteases by the Fungal Effector Pit2. *PLOS Pathol* **9**: e1003177
- O'Brien JA, Daudi A, Finch P, Butt VS, Whitelegge JP, Souda P, Ausubel FM, Bolwell GP** (2012) A Peroxidase-Dependent Apoplastic Oxidative Burst in Cultured *Arabidopsis* Cells Functions in MAMP-Elicited Defense. *Plant Physiol* **158**: 2013–2027
- Passardi F, Cosio C, Penel C, Dunand C** (2005) Peroxidases have more functions than a

- Swiss army knife. *Plant Cell Rep* **24**: 255–265
- Passardi F, Penel C, Dunand C** (2004) Performing the paradoxical: how plant peroxidases modify the cell wall. *Trends Plant Sci* **9**: 534–540
- Perrine-Walker FM, Gartner E, Hocart CH, Becker A, Rolfe BG** (2007) Rhizobium-initiated rice growth inhibition caused by nitric oxide accumulation. *Mol Plant Microbe Interact* **20**: 283–292
- Pitzschke A, Datta S, Persak H** (2014) Salt Stress in Arabidopsis: Lipid Transfer Protein AZI1 and Its Control by Mitogen-Activated Protein Kinase MPK3. *Mol Plant* **7**: 722–738
- Qi J, Wang J, Gong Z, Zhou JM** (2017) Apoplastic ROS signaling in plant immunity. *Curr Opin Plant Biol* **38**: 92–100
- Qiu H, Zhao X, Fang W, Wu H, Abubakar YS, Lu G, Wang Z, Zheng W** (2019) Spatiotemporal nature of *Fusarium graminearum*-wheat coleoptile interactions. *Phytopathol Res* **1**: 26
- Ralph J, Bunzel M, Marita JM, Hatfield RD, Lu F, Kim H, Schatz PF, Grabber JH, Steinhart H** (2004) Peroxidase-dependent cross-linking reactions of p-hydroxycinnamates in plant cell walls. *Phytochem Rev* **31**, **3**: 79–96
- Ren D, Yang H, Zhang S** (2002) Cell death mediated by MAPK is associated with hydrogen peroxide production in Arabidopsis. *J Biol Chem* **277**: 559–565
- Rudd JJ, Keon J, Hammond-Kosack KE** (2008) The wheat mitogen-activated protein kinases TaMPK3 and TaMPK6 are differentially regulated at multiple levels during compatible disease interactions with *Mycosphaerella graminicola*. *Plant Physiol* **147**: 802–815
- Sasaki K, Iwai T, Hiraga S, Kuroda K, Seo S, Mitsuhashi I, Miyasaka A, Iwano M, Ito H, Matsui H, et al.** (2004) Ten rice peroxidases redundantly respond to multiple stresses including infection with rice blast fungus. *Plant Cell Physiol* **45**: 1442–1452
- Schumacher J** (2012) Tools for *Botrytis cinerea*: New expression vectors make the gray mold fungus more accessible to cell biology approaches. *Fungal Genet Biol* **49**: 483–497
- Schwessinger B, Zipfel C** (2008) News from the frontline: recent insights into PAMP-triggered immunity in plants. *Curr Opin Plant Biol* **11**: 389–395

- Sewelam N, Kazan K, Schenk PM** (2016) Global Plant Stress Signaling: Reactive Oxygen Species at the Cross-Road. *Front Plant Sci* **7**: 187
- Sexauer M, Shen D, Schön M, Andersen TG, Markmann K** (2021) Visualizing polymeric components that define distinct root barriers across plant lineages. *Development* **148**: dev199820, doi:10.1242/dev.199820
- Smiley RW, Gourlie JA, Easley SA, Patterson LM, Whittaker RG** (2005) Crop damage estimates for crown rot of wheat and barley in the Pacific Northwest. *Plant Dis* **89**: 595-604
- Soler M, Serra O, Molinas M, Huguet G, Fluch S, Figueras M** (2007) A Genomic Approach to Suberin Biosynthesis and Cork Differentiation. *Plant Physiol* **144**: 419-431
- Sorokan AV, Kuluev BR, Burkhanova G, Maksimov IV** (2014) RNA silencing of the anionic peroxidase gene impairs potato plant resistance to *Phytophthora infestans* (Mont.) de Bary. *Mol Biol* **48**: 709–717
- Takáč T, Křenek P, Komis G, Vadovič P, Ovečka M, Ohnoutková L, Pechan T, Kašpárek P, Tichá T, Basheer J, et al.** (2021) TALEN-based HvMPK3 knock-Out attenuates proteome and root hair phenotypic responses to flg22 in barley. *Front Plant Sci* **12**: 666229
- Takáč T, Šamajová O, Luptovčíak I, Pechan T, Šamaj J** (2017) Feedback microtubule control and microtubule-actin cross-talk in *Arabidopsis* revealed by integrative proteomic and cell biology analysis of KATANIN 1 mutants. *Molec Cel Proteomics* **16**: 1591-1609
- Takáč T, Šamajová O, Vadovič P, Pechan T, Košútová P, Ovečka M, Husičková A, Komis G, Šamaj J** (2014) Proteomic and Biochemical Analyses Show a Functional Network of Proteins Involved in Antioxidant Defense of the *Arabidopsis* *anp2anp3* Double Mutant. *J Proteome Res* **13**: 5347–5361
- Takáč T, Vadovič P, Pechan T, Luptovčíak I, Šamajová O, Šamaj J** (2016) Comparative proteomic study of *Arabidopsis* mutants *mpk4* and *mpk6*. *Sci Rep* **6**: 28306
- Talbot NJ** (2019) Appressoria. *Curr Biol* **29**: R144–R146
- Tucker JR, Badea A, Blagden R, Pleskach K, Tittlemier SA, Fernando WGD** (2019) Deoxynivalenol-3-Glucoside Content Is Highly Associated with Deoxynivalenol Levels in Two-Row Barley Genotypes of Importance to Canadian Barley Breeding Programs. *Toxins (Basel)* **11**: 319

- Tucker JR, Legge WG, Maiti S, Hiebert CW, Simsek S, Yao Z, Xu W, Badea A, Fernando WGD** (2021) Transcriptome Alterations of an in vitro-Selected, Moderately Resistant, Two-Row Malting Barley in Response to 3ADON, 15ADON, and NIV Chemotypes of *Fusarium graminearum*. *Front Plant Sci* **12**: 1567
- Ursache R, Andersen TG, Marhavy P, Geldner N** (2018) A protocol for combining fluorescent proteins with histological stains for diverse cell wall components. *Plant J* **93**: 399–412
- Vogelgsang S, Beyer M, Pasquali M, Jenny E, Musa T, Bucheli TD, Wettstein FE, Forrer HR** (2019) An eight-year survey of wheat shows distinctive effects of cropping factors on different *Fusarium* species and associated mycotoxins. *Eur J Agron* **105**: 62–77
- Wang Q, Buxa SV, Furch A, Friedt W, Gottwald S** (2015) Insights Into *Triticum aestivum* Seedling Root Rot Caused by *Fusarium graminearum*. *Mol Plant Microbe Interact* **28**: 1288–1303
- Wang Q, Shao B, Shaikh FI, Friedt W, Gottwald S** (2018) Wheat Resistances to *Fusarium* Root Rot and Head Blight Are Both Associated with Deoxynivalenol- and Jasmonate-Related Gene Expression. *Phytopathol* **108**: 602–616
- Wojtasik W, Kulma A, Dymińska L, Hanuza J, Czemplik M, Szopa J** (2016) Evaluation of the significance of cell wall polymers in flax infected with a pathogenic strain of *Fusarium oxysporum*. *BMC Plant Biol* **16**: 75
- Xie K, Chen J, Wang Q, Yang Y** (2014) Direct Phosphorylation and Activation of a Mitogen-Activated Protein Kinase by a Calcium-Dependent Protein Kinase in Rice. *Plant Cell* **26**: 3077
- Xiong L, Yang Y** (2003) Disease Resistance and Abiotic Stress Tolerance in Rice Are Inversely Modulated by an Abscisic Acid-Inducible Mitogen-Activated Protein Kinase. *Plant Cell* **15**: 745–759
- Yang C, Fernando WGD** (2021) Analysis of the Oxidative Burst and Its Relevant Signaling Pathways in *Leptosphaeria maculans*—*Brassica napus* Pathosystem. *Int J Mol Sci* **22**: 4812
- Zhang W-J, Pedersen C, Kwaaitaal M, Gregersen PL, Mørch SM, Hanisch S, Kristensen A, Fuglsang AT, Collinge DB, Thordal-Christensen H** (2012) Interaction of barley

powdery mildew effector candidate CSEP0055 with the defence protein PR17c. *Mol Plant Pathol* **13**: 1110–1119

Zhang Y, Dong C (2007) Review Regulatory mechanisms of mitogen-activated kinase signaling. *Cell Mol Life Sci* **64**: 2771–2789

Figure legends

Figure 1. Colonization of root in barley wild type (WT) and *HvMPK3* KO lines by *Fusarium graminearum* mycelia 24h and 48h after inoculation with spores. (A-H) Overview of propidium iodide-labeled uninfected root apex of WT (A), *HvMPK3* KO-A (B), *HvMPK3* KO-B (C) and *HvMPK3* KO-D (D) lines under control conditions, and 24h after inoculation of roots with spores of GFP-expressing *F. graminearum* in WT (E), *HvMPK3* KO-A (F), *HvMPK3* KO-B (G) and *HvMPK3* KO-D (H) lines. Note red propidium iodide staining of cell walls in living cells and nuclei in dead cells. (I) Quantitative evaluation of the proportion of dead cells in control and infected root apices among tested barley lines. Data are presented as means \pm SD; n = 20 roots/line, 70-90 epidermal cells evaluated in each root, error bars represent standard deviations. Different lowercase letters above the error bars (I) represent statistical significance according to one-way ANOVA and subsequent LSD test at p value < 0.05. (J-M) Roots of WT (J), *HvMPK3* KO-A (K), *HvMPK3* KO-B (L) and *HvMPK3* KO-D (M) lines stained with propidium iodide 48h after inoculation with spores of GFP-expressing *F. graminearum*. Hyphae growing on root surface in parallel orientation with elongated root epidermal cells are indicated by white arrows, hyphae growing away and not touching roots are indicated by yellow arrows, zones occupied by malformed mycelia with wavy growth pattern, growing perpendicularly to elongated root epidermal cells are indicated by asterisks. Scale bars: 50 μ m (A-H) and 100 μ m (J-M).

Figure 2. Comparison of root phenotypes in barley wild type (WT) and *HvMPK3* KO lines between non-treated and *Fusarium graminearum*-treated plants 10 days after inoculation with spores. (A-H) Morphology of roots in the basal part of the root system of the uninfected plant of WT (A), *HvMPK3* KO-A (B), *HvMPK3* KO-B (C) and *HvMPK3* KO-D (D) lines under control conditions, and 10 days after inoculation in WT (E), *HvMPK3* KO-A (F), *HvMPK3*

KO-B (G) and *HvMPK3* KO-D (H) lines. The extent of infection and the rate of root damage is indicated by a reddish-brown coloration originating from the *F. graminearum* mycelia. Note apparent morphological changes in roots of WT (E, arrowheads) that are not present in roots of *HvMPK3* KO-A (F), *HvMPK3* KO-B (G) and *HvMPK3* KO-D (H) lines. Uncropped original images of the tested barley plants are presented in Figure S3. Scale bars: 1 cm. (I) Quantitative evaluation of the root length in WT and *HvMPK3* KO lines without infection (Control), and 10 days after infection with *F. graminearum* spores (with Fusarium). Data are presented as means \pm SD; n = 30 plants/line, error bars represent standard deviations. Different lowercase letters above the error bars (I) represent statistical significance according to one-way ANOVA and subsequent LSD test at p value < 0.05 .

Figure 3. Visualization of volumetric fluorescence signal distribution of *F. graminearum* hyphae growing on root surface of barley wild type (WT) and *HvMPK3* KO lines 48h after inoculation with spores. Depth of the hyphae localization is indicated by a color-coding depicted on the root surface by blue color and deep inside the root tissue by red color. The color range in each image is indicated in μm . (A, B) Formation of appressoria (yellow arrows) and infection hyphae (white arrows) penetrating cell wall of epidermal cells in roots of WT plants. Inset in (B) shows detailed 3D visualization of appressorium (yellow arrows) and infection hyphae (white arrows). (C-H) Developed mycelia on root surface of *HvMPK3* KO-A (C, D), *HvMPK3* KO-B (E, F) and *HvMPK3* KO-D (G, H) lines. Appressoria are indicated by yellow arrows, cell wall penetration and formation of infection hyphae were not detected by color-coded analysis. Scale bars: 10 μm (A, B) and 20 μm (C-H).

Figure 4. Morphology of *F. graminearum* appressoria, their number and the mycelium penetration potential on root surface of barley wild type (WT) and *HvMPK3* KO lines 48h after inoculation with spores. (A-D) Mycelium density and the appressoria morphology 48h after inoculation with *F. graminearum* spores on the root surface of WT (A), *HvMPK3* KO-A (B), *HvMPK3* KO-B (C) and *HvMPK3* KO-D (D) lines. Appressoria are indicated by yellow arrows. Scale bars: 20 μm . (E) Quantitative evaluation of the average number of appressoria developed on the surface of infected roots. (F) Quantitative evaluation of the average number of the penetration events on the surface of infected roots. Data are represented

as mean \pm SD; n = 10 images/line, error bars represent standard deviations. Different lowercase letters above the error bars represent statistical significance according to one-way ANOVA and subsequent LSD test at p value < 0.05 .

Figure 5. Fluorescence detection of ROS production in roots of barley wild type (WT) and *HvMPK3* KO lines 24h after inoculation with *Fusarium graminearum* spores. (A-D) Overview of the root apex labeled by CM-H₂DCFDA probe 24h after inoculation in WT (A), *HvMPK3* KO-A (B), *HvMPK3* KO-B (C) and *HvMPK3* KO-D (D) lines. (E) Quantitative evaluation of the fluorescence intensity after CM-H₂DCFDA labeling of control and inoculated roots. Quantification was performed 24h after inoculation with *F. graminearum*. Data are presented as means \pm SD; n = 15 plants/line, error bars represent standard deviations. Different lowercase letters above the error bars represent statistical significance according to one-way ANOVA and subsequent LSD test at p value < 0.05 . (F) Increased ROS production in root epidermal cells of WT plant treated with mCherry-expressing *F. graminearum* (white arrows) for 24h. Note the close contact of ROS-producing cell and the mycelia (white arrowhead) before infection. (G-J) Local view of the infected root zone 24h after inoculation with GFP-expressing *F. graminearum* and subsequently labeled by CM-H₂DCFDA for ROS and by propidium iodide for cell walls in living cells and for nuclei in dead cells in WT (G), *HvMPK3* KO-A (H), *HvMPK3* KO-B (I) and *HvMPK3* KO-D (J) lines. Scale bars: 1 mm (A-D), 50 μ m (G-J), 10 μ m (F).

Figure 6. Heat map depicting the fold changes of defence-related proteins, histones, and proteins involved in redox regulation differentially regulated in WT and *HvMPK3* KO plants in response to *Fusarium graminearum* (this study) and flagellin 22 (flg22) treatment (Takáč et al., 2021). Fold changes are presented in color as indicated by the color key on the right. Proteins unique for either control or treated samples were found solely in the proteomes of control or treated samples, considering all analyzed replicates. JA = jasmonic acid; PR = pathogenesis related proteins; PRX = peroxidases; LTPs = lipid transfer proteins.

Figure 7. Heat map depicting the fold changes of protein involved in protein degradation, abiotic stress response, cell wall modification, membrane transport and cytoskeleton,

differentially regulated in WT and *HvMPK3* KO plants in response to *Fusarium graminearum* (this study) and flagellin 22 (flg22) treatment (Takáč et al., 2021). Fold changes are presented in color as indicated by the color key on the right. Proteins unique for either control or treated samples were found solely in the proteomes of control or treated samples, considering all analyzed replicates.

Figure 8. Specific activity of peroxidases and abundances of ascorbate peroxidase and catalase in roots of barley wild type (WT) and *HvMPK3* KO lines (KO-A and KO-B) 24h after inoculation with *Fusarium graminearum*. (A) Images of native polyacrylamide gels showing activity of peroxidases. (B) Graphs showing quantifications of band optical intensities in (A). (C, E, G) Immunoblotting analyses of cytosolic ascorbate peroxidase (cAPX; C), catalase (E) and pathogenesis related protein 1 (*HvPR-1*; G). (D, F, H) Graphs showing quantifications of band optical intensities in (C, E and G). Data are presented as means \pm SD; error bars represent standard deviations. Asterisks above the error bars represent statistical significant differences between control and treated samples according to Student's t-test at p value < 0.05 . Uncropped, full original images of the gels are documented in Figure S8.

Figure 9. Suberin staining of barley roots 24h after inoculation with *Fusarium graminearum* spores. Freehand cross-sections of roots were stained with fluorescent suberin dye Fluorol Yellow 088 under control conditions (upper panel) and 24h after inoculation with *F. graminearum* spores (lower panel). (A, B) wild type, (C, D) *HvMPK3* KO-A line and (E, F) *HvMPK3* KO-B line. Note strongly increased suberin staining in surface cell layers, endodermis and xylem of both *HvMPK3* KO lines. (G) Quantification of suberin staining in freehand barley root cross-sections. Asterisks indicate statistically significant differences between control and treated samples of appropriate line, * $p < 0.05$, ** $p < 0.01$, Student's t-test. Scale bars: 50 μm .

Figure 10. Lignin staining of barley roots 24h after inoculation with *Fusarium graminearum* spores. Freehand cross-sections of roots were stained with fluorescent lignin dye Basic Fuchsin under control conditions (upper panel) and 24h after inoculation with *F. graminearum* spores (lower panel). (A, B) wild type, (C, D) *HvMPK3* KO-A line and (E, F) *HvMPK3* KO-B line. Note strongly increased suberin staining in surface cell layers,

endodermis and xylem of both *HvMPK3* KO lines. **(G)** Quantification of suberin staining in freehand barely root cross-sections. Asterisks indicate statistically significant differences between control and treated samples of appropriate line, ** $p < 0.01$, *** $p < 0.001$, Student's t-test. Scale bars: 50 μm .

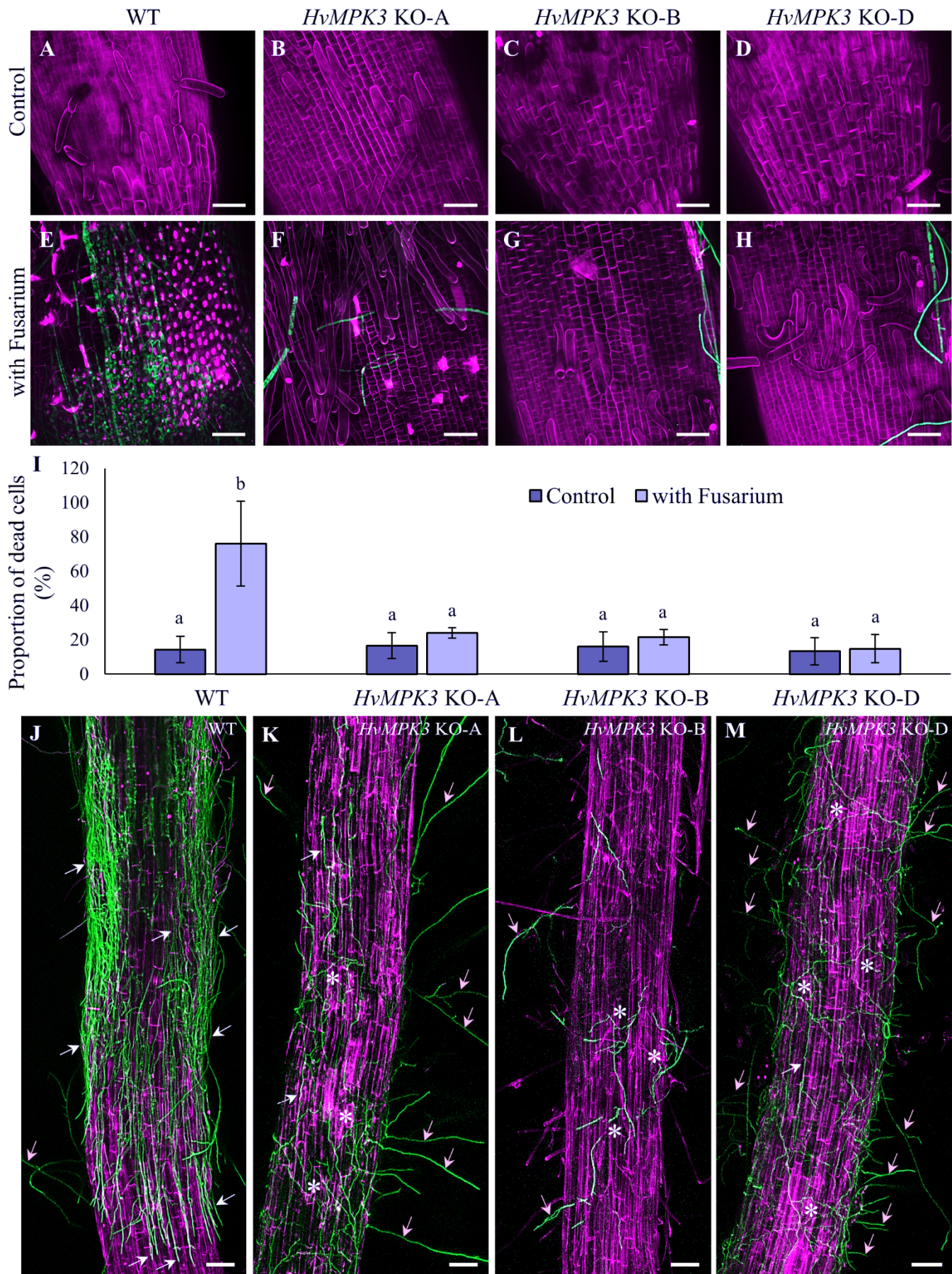


Figure 1. Colonization of root in barley wild type (WT) and *HvMPK3* KO lines by *Fusarium graminearum* mycelia 24h and 48h after inoculation with spores. (A-H) Overview of propidium iodide-labeled uninfected root apex of WT (A), *HvMPK3* KO-A (B), *HvMPK3* KO-B (C) and *HvMPK3* KO-D (D) lines under control conditions, and 24h after inoculation of roots with spores of GFP-expressing *F. graminearum* in WT (E), *HvMPK3* KO-A (F), *HvMPK3* KO-B (G) and *HvMPK3* KO-D (H) lines. Note red propidium iodide staining of cell walls in living cells and nuclei in dead cells. (I) Quantitative evaluation of the proportion of dead cells in control and infected root apices among tested barley lines. Data are presented as means \pm SD; n = 20 roots/line, 70-90 epidermal cells evaluated in each root, error bars represent standard deviations. Different lowercase letters above the error bars (I) represent statistical significance according to one-way ANOVA and subsequent LSD test at p value < 0.05. (J-M) Roots of WT (J), *HvMPK3* KO-A (K), *HvMPK3* KO-B (L) and *HvMPK3* KO-D (M) lines stained with propidium iodide 48h after inoculation with spores of GFP-expressing *F. graminearum*. Hyphae growing on root surface and in parallel with elongated root epidermal cells are indicated by white arrows, hyphae growing away and not touching roots are indicated by yellow arrows, zones occupied by malformed mycelia with wavy growth pattern, growing perpendicularly to elongated root epidermal cells are indicated by asterisks. Scale bars: 50 μ m (A-H) and 100 μ m (J-M).

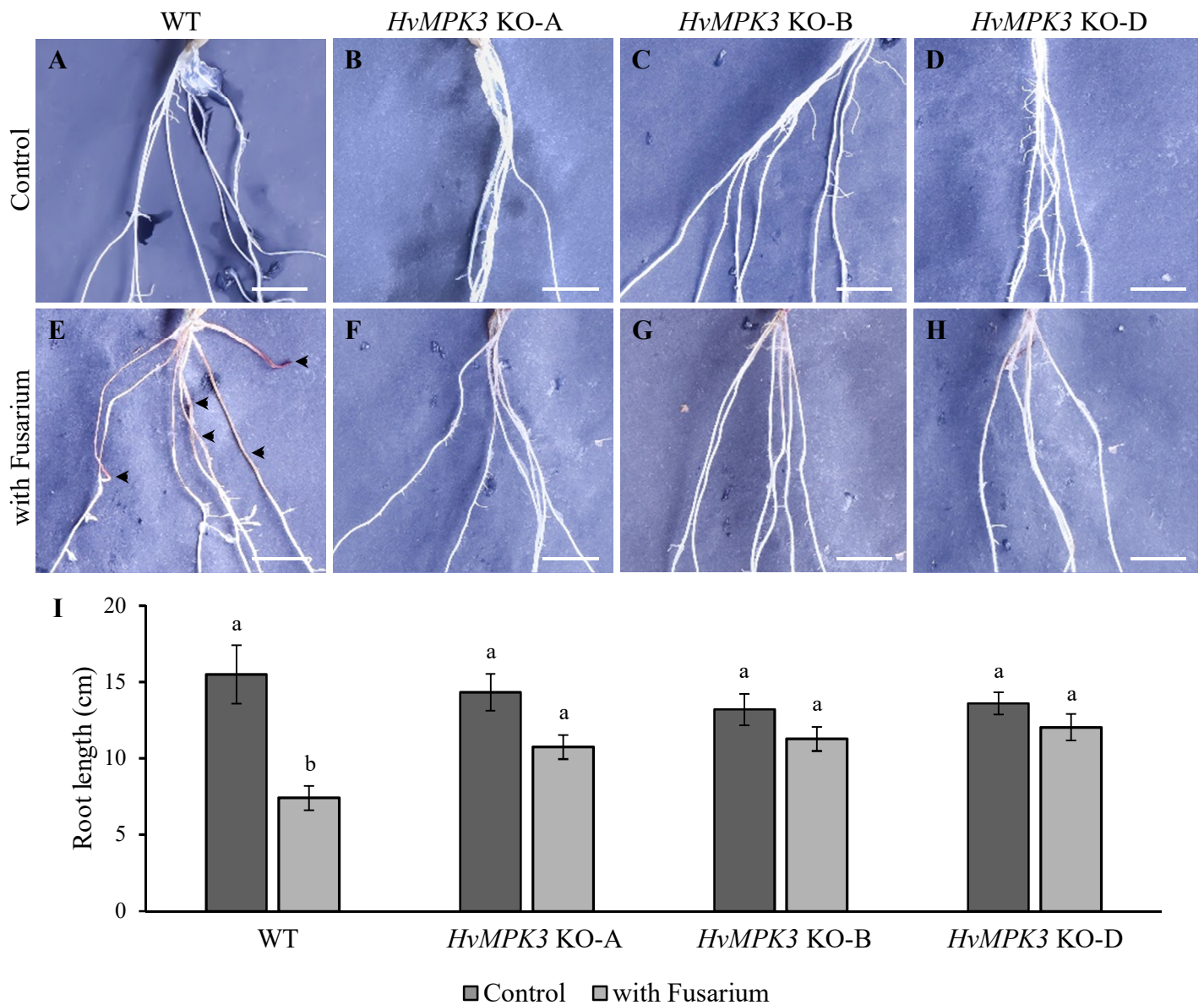


Figure 2. Comparison of root phenotypes in barley wild type (WT) and *HvMPK3* KO lines between non-treated and *Fusarium graminearum*-treated plants 10 days after inoculation with spores. (A-H) Morphology of roots in the basal part of the root system of the uninfected plant of WT (A), *HvMPK3* KO-A (B), *HvMPK3* KO-B (C) and *HvMPK3* KO-D (D) lines under control conditions, and 10 days after inoculation in WT (E), *HvMPK3* KO-A (F), *HvMPK3* KO-B (G) and *HvMPK3* KO-D (H) lines. The extent of infection and the rate of root damage is indicated by a reddish-brown coloration originating from the *F. graminearum* mycelia. Note apparent morphological changes in roots of WT (E, arrowheads) that are not present in roots of *HvMPK3* KO-A (F), *HvMPK3* KO-B (G) and *HvMPK3* KO-D (H) lines. Uncropped original images of the tested barley plants are presented in Figure S2. Scale bars: 1 cm. (I) Quantitative evaluation of the root length in WT and *HvMPK3* KO lines without infection (Control), and 10 days after infection with *F. graminearum* spores (with Fusarium). Data are presented as means \pm SD; n = 30 plants/line, error bars represent standard deviations. Different lowercase letters above the error bars (I) represent statistical significance according to one-way ANOVA and subsequent LSD test at p value < 0.05.

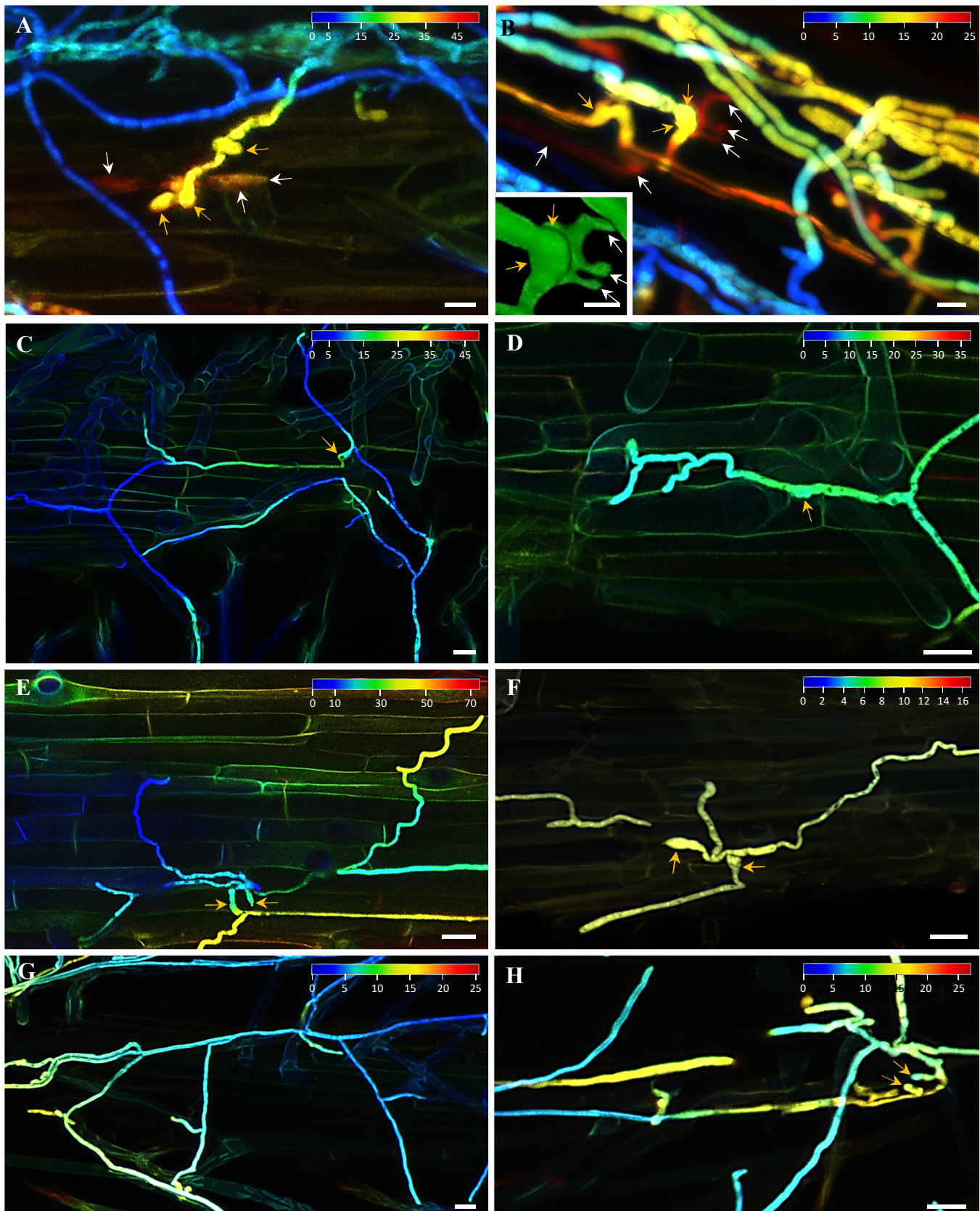


Figure 3. Visualization of volumetric fluorescence signal distribution of *F. graminearum* hyphae growing on root surface of barley wild type (WT) and *HvMPK3* KO lines 48h after inoculation with spores. Depth of the hyphae localization is indicated by a color-coding depicted on the root surface by blue color and deep inside the root tissue by red color. The color range in each image is indicated in μm . (A, B) Formation of appressoria (yellow arrows) and infection hyphae (white arrows) penetrating cell wall of epidermal cells in roots of WT plants. Inset in (B) shows detailed 3D visualization of appressorium (yellow arrows) and infection hyphae (white arrows). (C-H) Developed mycelia on root surface of *HvMPK3* KO-A (C, D), *HvMPK3* KO-B (E, F) and *HvMPK3* KO-D (G, H) lines. Appressoria are indicated by yellow arrows, cell wall penetration and formation of infection hyphae were not detected by color-coded analysis. Scale bars: 10 μm (A, B) and 20 μm (C-H).

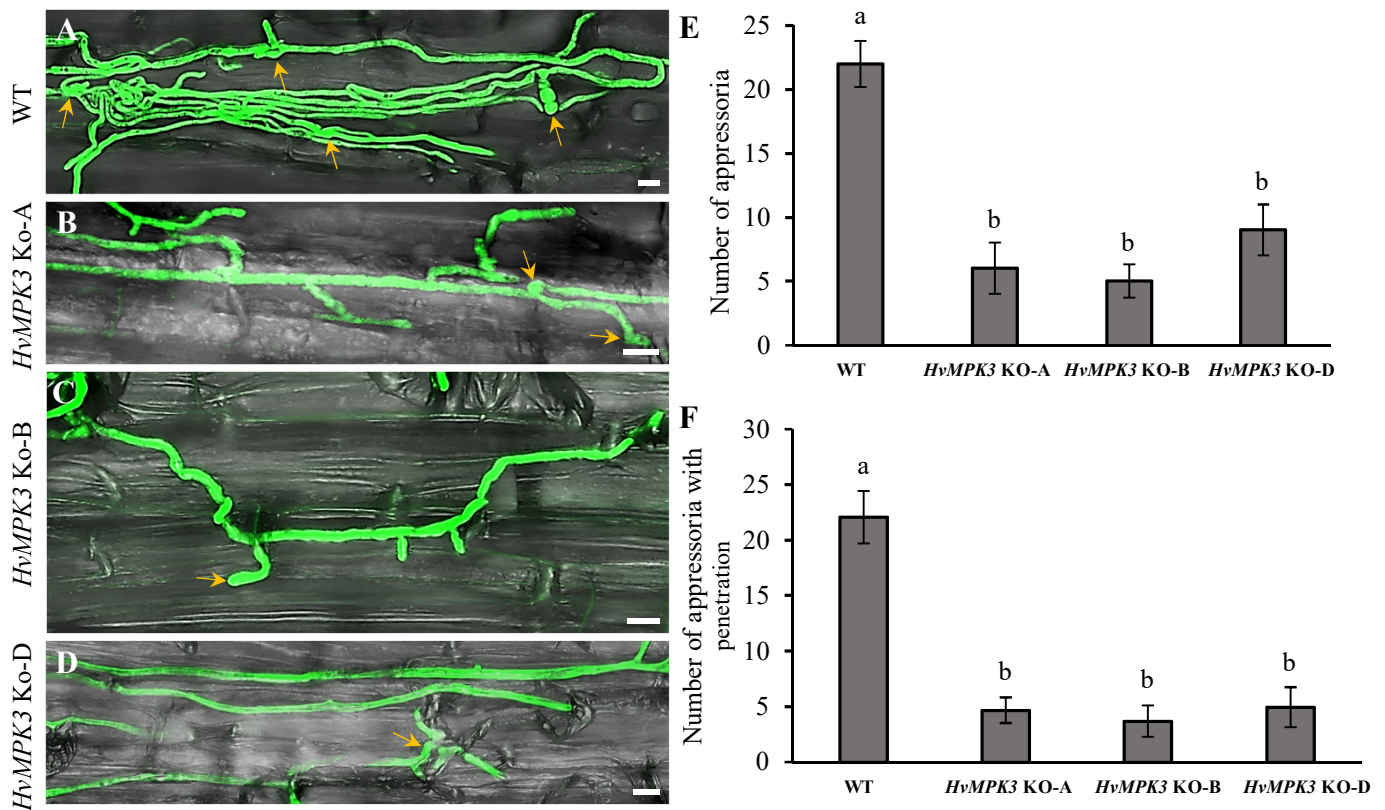


Figure 4. Morphology of *F. graminearum* appressoria, their number and the mycelium penetration potential on root surface of barley wild type (WT) and *HvMPK3* KO lines 48h after inoculation with spores. (A-D) Mycelium density and the appressoria morphology 48h after inoculation with *F. graminearum* spores on the root surface of WT (A), *HvMPK3* KO-A (B), *HvMPK3* KO-B (C) and *HvMPK3* KO-D (D) lines. Appressoria are indicated by yellow arrows. Scale bars: 20μm. (E) Quantitative evaluation of the average number of appressoria developed on the surface of infected roots. (F) Quantitative evaluation of the average number of the penetration events on the surface of infected roots. Data are represented as mean ± SD; n = 10 images/line, error bars represent standard deviations. Different lowercase letters above the error bars represent statistical significance according to one-way ANOVA and subsequent LSD test at p value < 0.05.

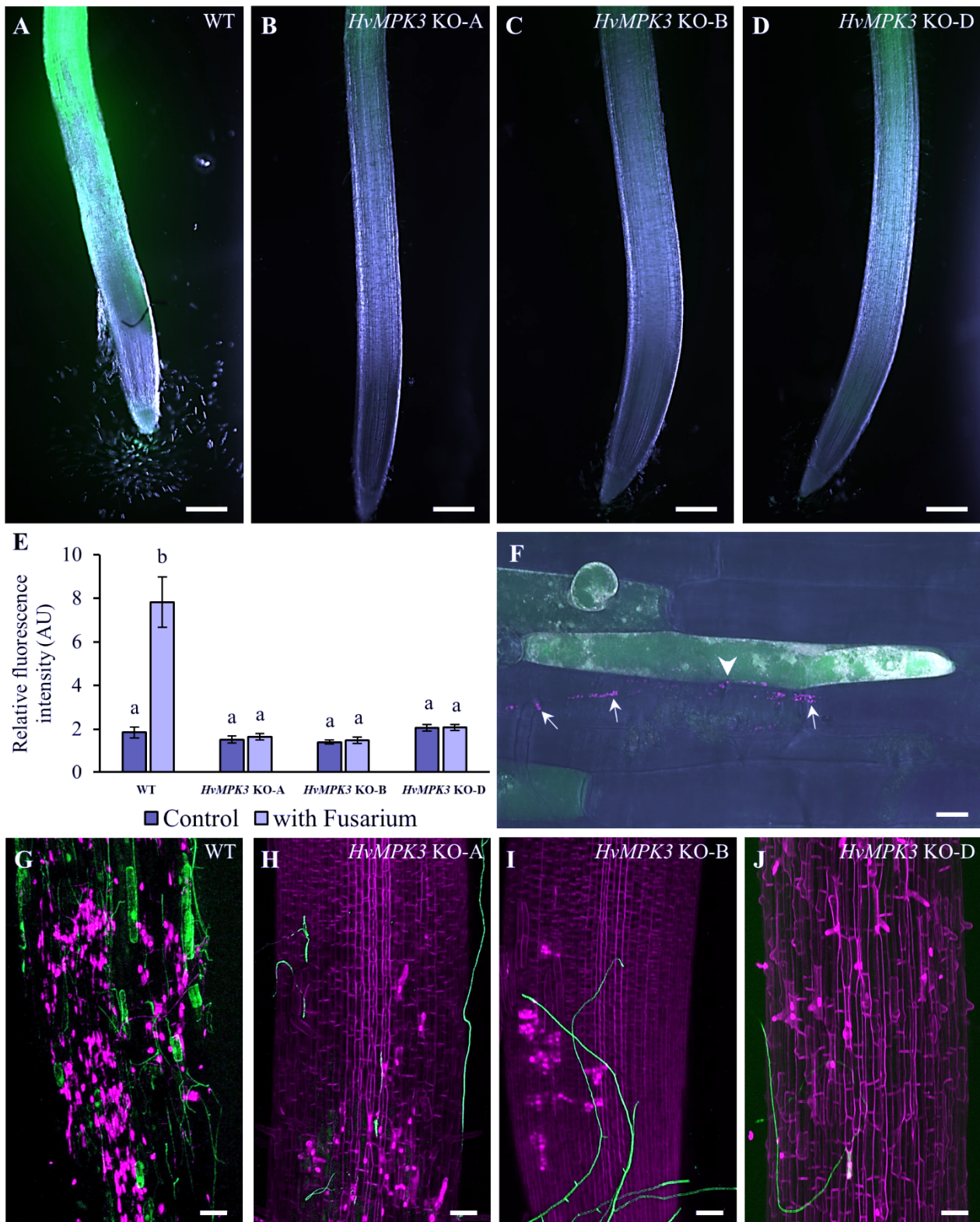


Figure 5. Fluorescence detection of ROS production in roots of barley wild type (WT) and *HvMPK3* KO lines 24h after inoculation with *Fusarium graminearum* spores. (A-D) Overview of the root apex labeled by CM-H₂DCFDA probe 24h after inoculation in WT (A), *HvMPK3* KO-A (B), *HvMPK3* KO-B (C) and *HvMPK3* KO-D (D) lines. **(E)** Quantitative evaluation of the fluorescence intensity after CM-H₂DCFDA labeling of control and inoculated roots. Quantification was performed 24h after inoculation with *F. graminearum*. Data are presented as means ± SD; n = 15 plants/line, error bars represent standard deviations. Different lowercase letters above the error bars represent statistical significance according to one-way ANOVA and subsequent LSD test at *p* value < 0.05. **(F)** Increased ROS production in root epidermal cells of WT plant treated with mCherry-expressing *F. graminearum* (white arrows) for 24h. Note the close contact of ROS-producing cell and the mycelia (white arrowhead) before infection. **(G-J)** Local view of the infected root zone 24h after inoculation with GFP-expressing *F. graminearum* and subsequently labeled by CM-H₂DCFDA for ROS and by propidium iodide for cell walls in living cells and for nuclei in dead cells in WT (G), *HvMPK3* KO-A (H), *HvMPK3* KO-B (I) and *HvMPK3* KO-D (J) lines. Scale bars: 1 mm (A-D), 50 μm (G-J), 10 μm (F).

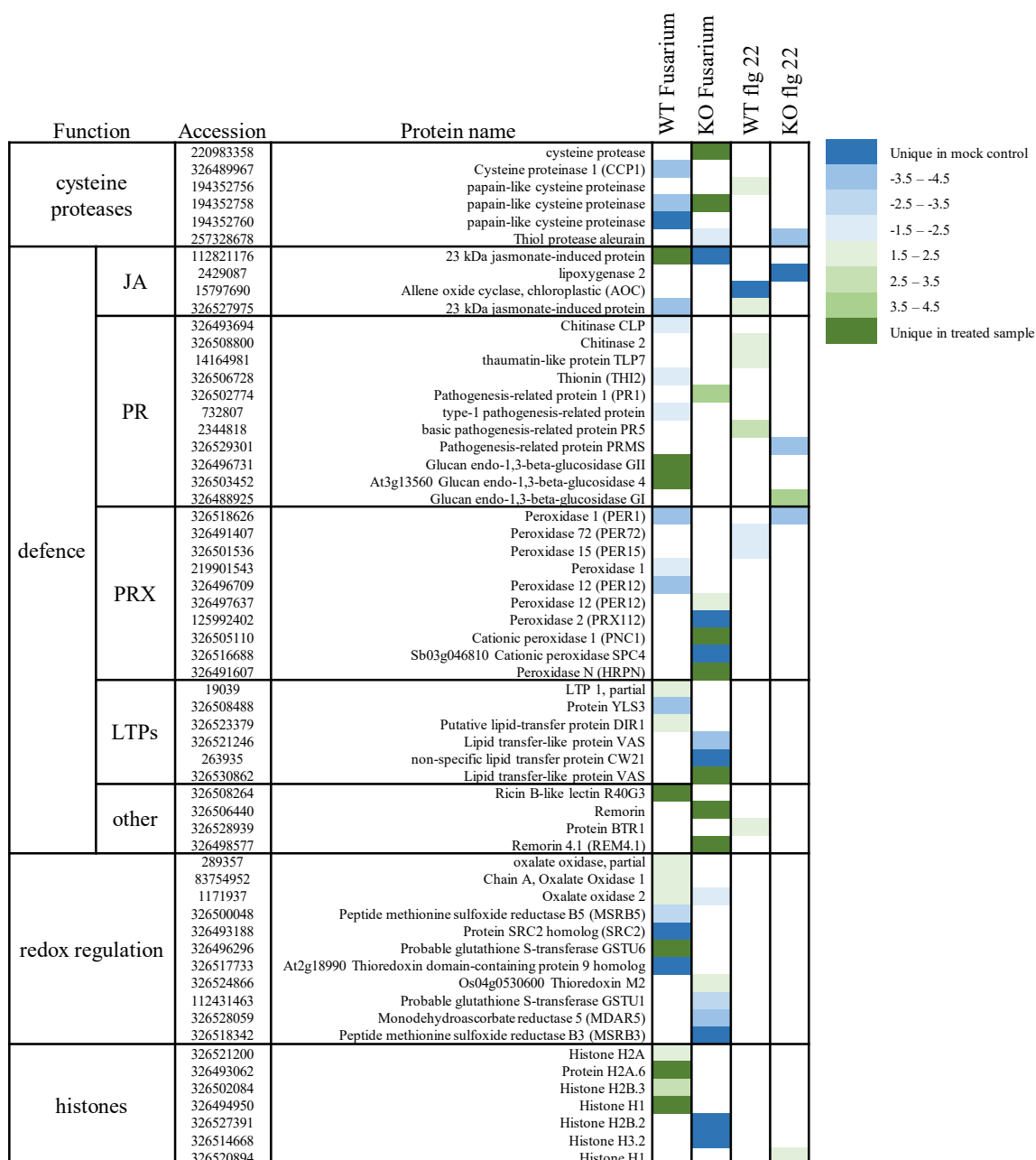


Figure 6. Heat map depicting the fold changes of defence related proteins, histones, and proteins involved in redox regulation differentially regulated in WT and *HvMPK3* KO plants in response to *Fusarium graminearum* inoculation (this study) and flagellin 22 (flg22) treatment (Takáč *et al.*, 2021). Fold changes are presented in color as indicated by the color key on the right. Proteins unique for either control or treated samples were found solely in the proteomes of control or treated samples, considering all analyzed replicates. JA = jasmonic acid; PR = pathogenesis related proteins; PRX = peroxidases; LTPs = lipid transfer proteins.

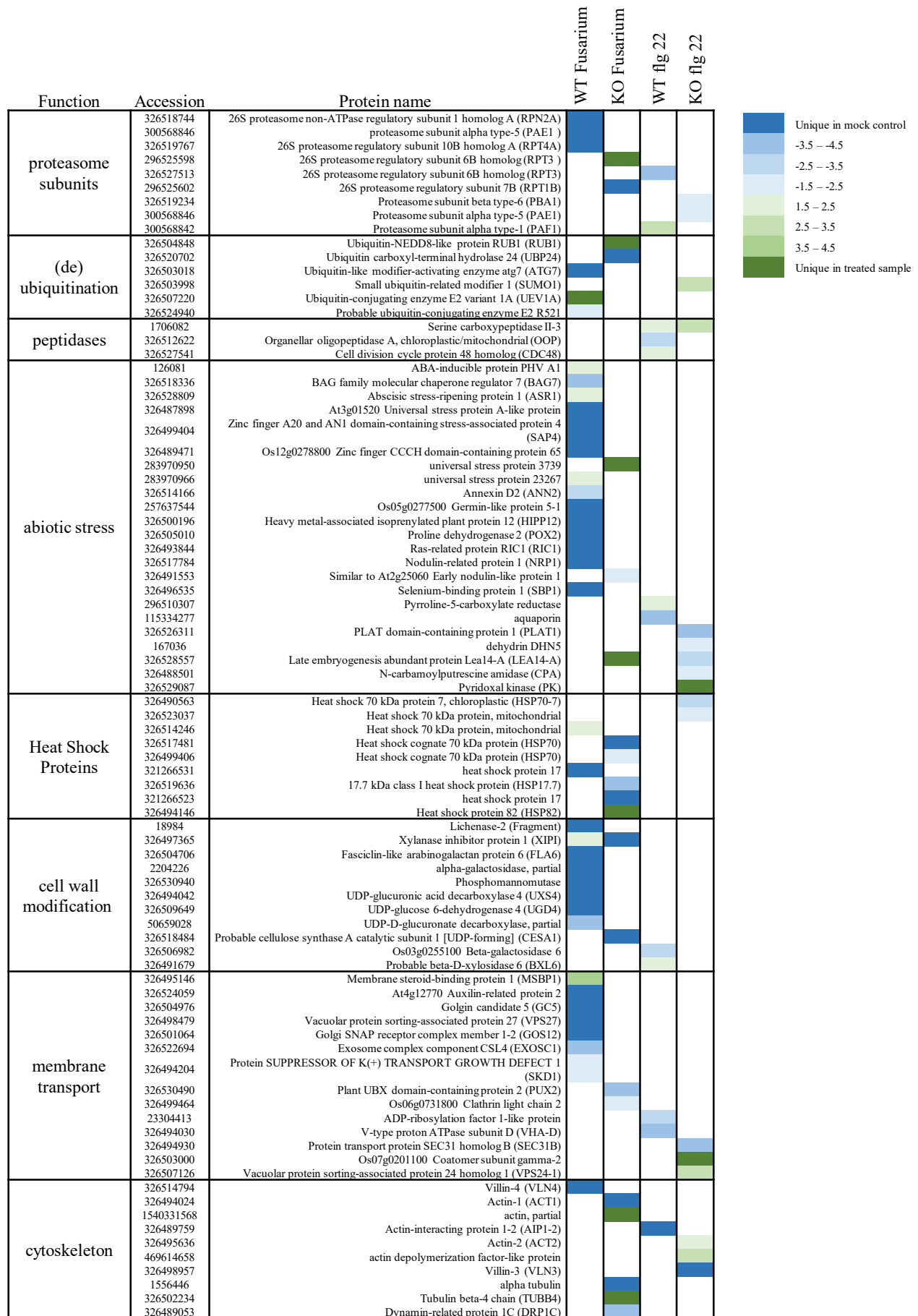


Figure 7. Heat map depicting the fold changes of protein involved in protein degradation, abiotic stress response, cell wall modification, membrane transport and cytoskeleton, differentially regulated in WT and *HvMPK3* KO plants in response to *Fusarium graminearum* inoculation (this study) and flagellin 22 (flg22) treatment (Takáč *et al.*, 2021). Fold changes are presented in color as indicated by the color key on the right. Proteins unique for either control or treated samples were found solely in the proteomes of control or treated samples, considering all analyzed replicates.

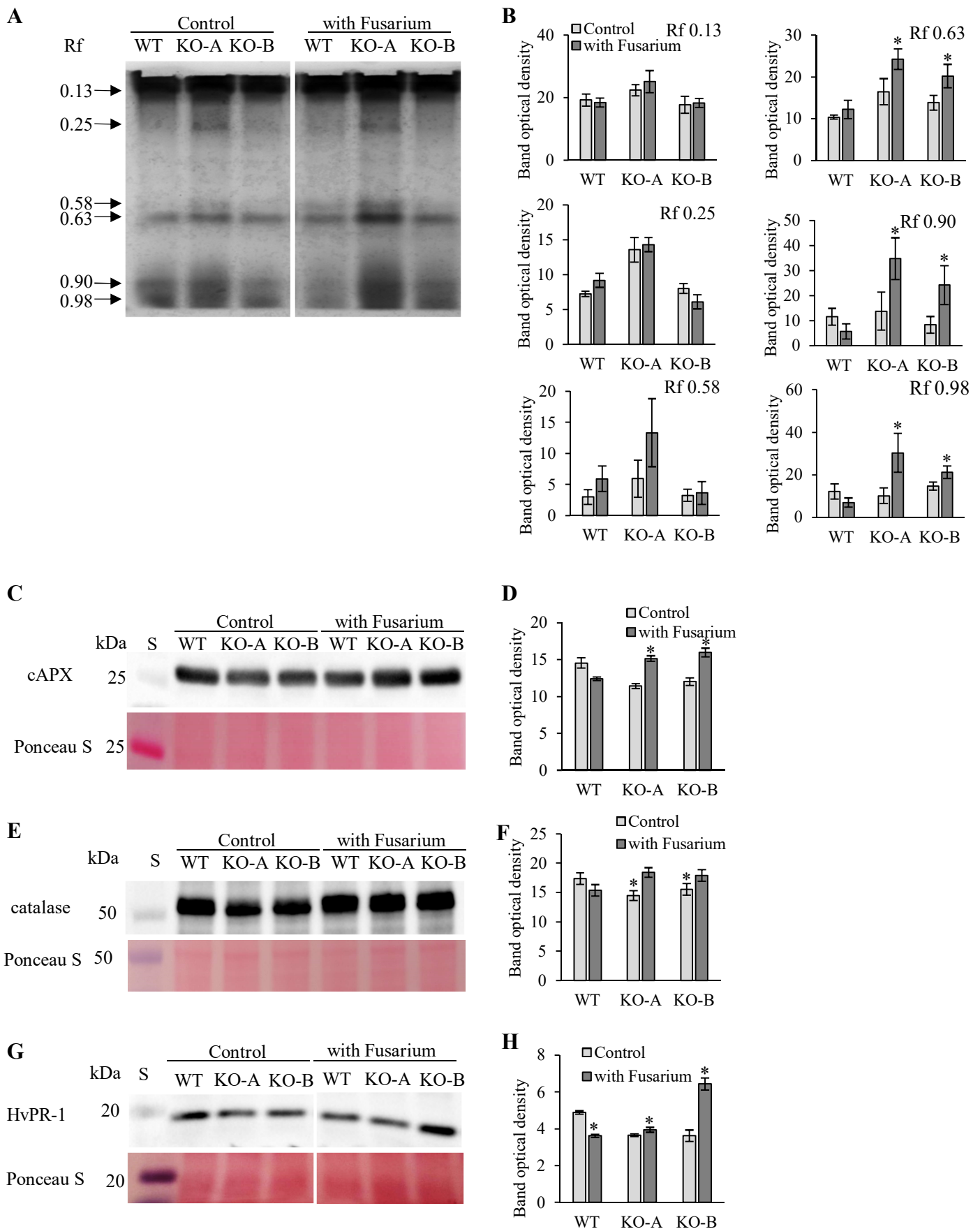


Figure 8. Specific activity of peroxidases and abundances of ascorbate peroxidase and catalase in roots of barley wild type (WT) and *HvMPK3* KO lines (KO-A and KO-B) 24h after inoculation with *Fusarium graminearum*. (A) Images of native polyacrylamide gels showing activity of peroxidases. (B) Graphs showing quantifications of band optical intensities in (A). (C, E, G) Immunoblotting analyses of cytosolic ascorbate peroxidase (cAPX; C), catalase (E) and pathogenesis related protein 1 (HvPR-1; G). (D, F, H) Graphs showing quantifications of band optical intensities in (C, E and G). Data are presented as means \pm SD; error bars represent standard deviations. Asterisks above the error bars represent statistical significant differences between control and treated samples according to Student's t-test at p value $<$ 0.05. Uncropped, full original images of the gels are documented in Figure S8.

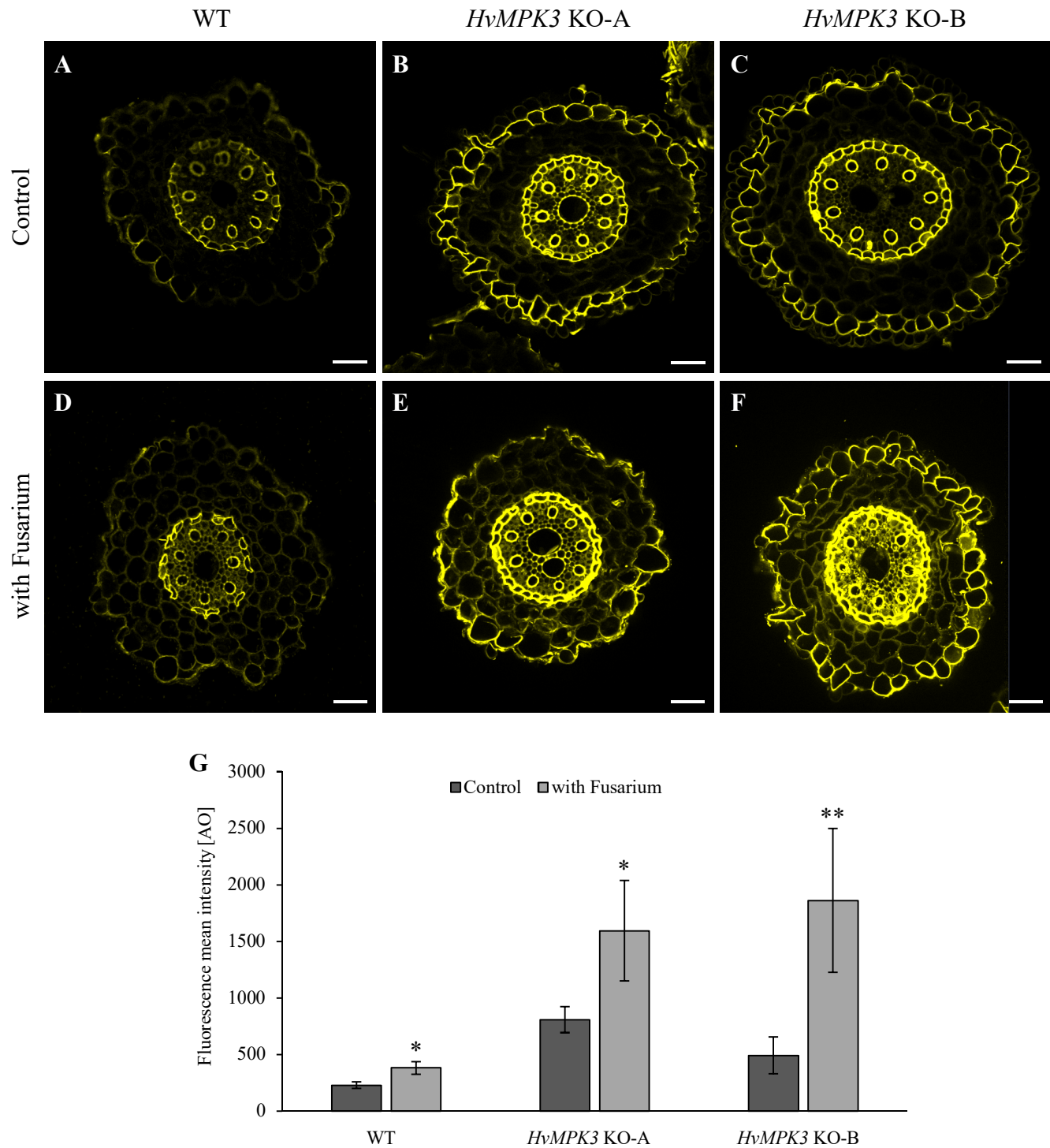


Figure 9. Suberin staining of barley roots 24h after inoculation with *Fusarium graminearum* spores. Freehand cross-sections of roots were stained with fluorescent suberin dye Fluorol Yellow 088 under control conditions (upper panel) and 24h after inoculation with *Fusarium graminearum* spores (lower panel). (A, B) wild type, (C, D) *HvMPK3* KO-A line and (E, F) *HvMPK3* KO-B line. Note strongly increased suberin staining in surface cell layers, endodermis and xylem of both *HvMPK3* KO lines. (G) Quantification of suberin staining in freehand barley root cross-sections. Asterisks indicate statistically significant differences between control and treated samples of appropriate line, * p<0.05, ** p<0.01, Student's t-test. Scale bars: 50 μ m.

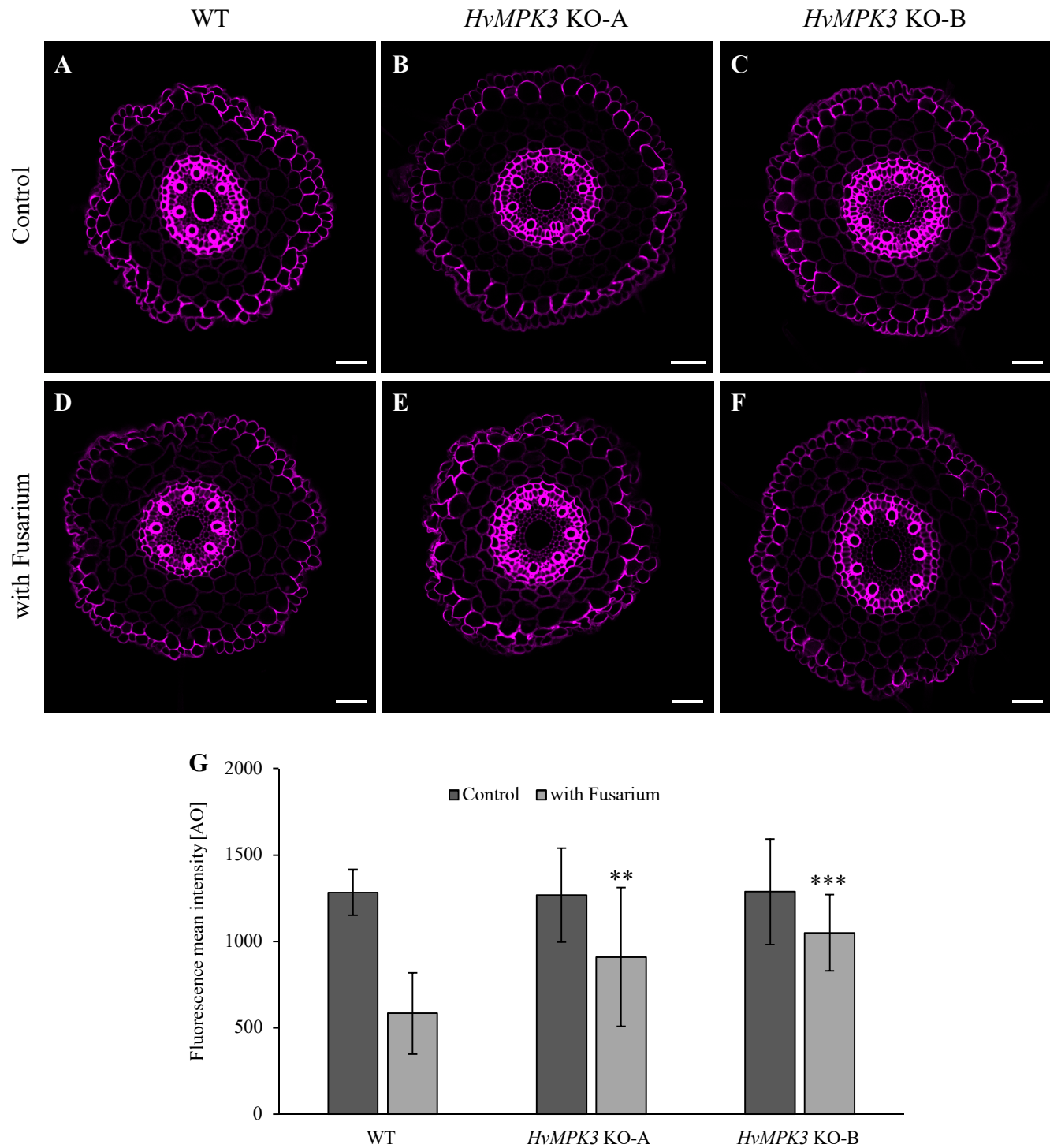


Figure 10. Lignin staining of barley roots 24h after inoculation with *Fusarium graminearum* spores. Freehand cross-sections of roots were stained with fluorescent lignin dye Basic Fuchsin under control conditions (upper panel) and 24 h after inoculation with *F. graminearum* spores (lower panel). (A, B) wild type, (C, D) *HvMPK3* KO-A line and (E, F) *HvMPK3* KO-B line. Note strongly increased suberin staining in surface cell layers, endodermis and xylem of both *HvMPK3* KO lines. (G) Quantification of suberin staining in freehand barley root cross-sections. Asterisks indicate statistically significant differences between control and treated samples of appropriate line, ** $p < 0.01$, *** $p < 0.001$, Student's t-test. Scale bars: 50 μm .